EFFECT OF THROUGH-THE-THICKNESS STITCHING ON POST-BUCKLING AND IMPACT RESPONSE OF COMPOSITE LAMINATES

By

HUASHENG ZHU

A DISSERTATION PRESENTED TO THE GRADUATE SCHOOL
OF THE UNIVERSITY OF FLORIDA IN PARTIAL FULFILLMENT
OF THE REQUIREMENTS FOR THE DEGREE OF
DOCTOR OF PHILOSOPHY

UNIVERSITY OF FLORIDA

1995

To my parents Deqian Zhu and Guirong Liu
and my beloved Ying-Feng Liu

ACKNOWLEDGMENTS

The author would like to express her sincere gratitude to her advisor, Dr. Bhavani V. Sankar, for his patient guidance, constant encouragement, and endless support of her study.

The author is also grateful to Dr. Nicolae D. Cristescu, Dr. Peter G. Ifju, Dr. Edward K. Walsh, and Dr. Reynaldo Roque for serving as her committee members.

Finally the author would like to express her gratitude to her parents, brothers, and her love, Mr. Ying-Feng Lau, who share the happiness, sadness, difficulty with the author, for their encouragement, support, and patience.

TABLE OF CONTENTS

Page

ACKNOWLEDGMENTS ii

ABSTRACT v

CHAPTERS

1 INTRODUCTION AND LITERATURE REVIEW 1

1.1 Background
1.2 Literature Review 3
1.2.1 Research on Post-buckling of Delaminate Composite 4
1.2.2 Research on Low Velocity Impact Response and Damage of Delaminated Composite Materials 9
1.2.3 Research Related to Delaminated Composite Materials with Stitches 11
1.3 Objectives and Scope of the Present Study 16

2 AN ANALYTICAL SOLUTION FOR POST-BUCKLING OF A DELAMINATED COMPOSITE BEAM WITH STITCHING 18

2.1 Basic Assumptions 19
2.2 Analytical Model 20
2.2.1 Delaminated Composite Beam without Stitching 20
2.2.2 Delaminated Beam with Through-the-Thickness Stitches 28
2.3 Results and Discussion 34

3 FINITE ELEMENT ANALYSIS OF A DELAMINATED COMPOSITE WITH STITCHING 44

3.1 Specimen 45
3.2 Finite Element Model 46
3.3 Post-Buckling Analysis 50
3.4 Energy Release Rate 52
3.5 Results and Discussion 55

4 EFFECT OF STITCHING ON LOW-VELOCITY IMPACT RESPONSE .73

4.1 Basic Assumptions 73
4.2 Analytical Model 75
    4.2.1 Relation between Contact Force and Beam Deflection 76
    4.2.2 Impact Response 85
4.3 Numerical Examples, Results, and Discussion 88

5 CONCLUSIONS AND FUTURE WORK 101

5.1 Summary 101
5.2 Suggestions for Future Work 103

APPENDIX DERIVATION OF FORCE DISPLACEMENT RELATIONS IN THE BEAM ELEMENT 104

REFERENCES 112

BIOGRAPHICAL SKETCH 119

Abstract of Dissertation Presented to the Graduate School
of the University of Florida in Partial Fulfillment of the
Requirements for the Degree of Doctor of Philosophy

EFFECT OF THROUGH-THE-THICKNESS STITCHING ON POST-BUCKLING AND IMPACT RESPONSE OF COMPOSITE LAMINATES

By

Huasheng Zhu

December 1999

Chairman: Bhavani V. Sankar
Major Department: Aerospace Engineering, Mechanics, and Engineering Science

Fiber composite materials have very high specific strength and stiffness. This structural efficiency enables composite materials to be used in a wide variety of applications. However, laminated composites have also some disadvantages such as poor inter-laminar strength, low impact resistance, and poor delamination resistance. During the manufacture of fiber-reinforced composite laminates, imperfections can cause initial delamination, and the impact on laminated composites by foreign objects during service can cause delamination propagation. Delamination is one of the most dominant forms of damage due to lack of reinforcement in the thickness direction. An effective

method to provide this reinforcement is to use through-the-thickness stitching.

When the delaminated composite is under compression, it may undergo post-buckling. When the energy release rate is greater than critical energy release rate, the delamination will propagate in an unstable manner and finally cause catastrophic failure of the composite. In this dissertation analytical and finite element methods are proposed to investigate the effect of through-the-thickness stitching on the post-buckling of a delaminated composite. In particular the studies focus on the effect of stitching on buckling load, load-displacement behavior, and energy release rate.

When a delaminated composite is subject to a low-velocity impact, the crack may propagate and finally cause catastrophic failure. In this dissertation an analytical model is proposed to understand the effect of stitching on improving impact damage resistance. In particular the studies focus on the effects of stitching when the impact energy, delamination length and location, and the fracture toughness are varied.

CHAPTER 1

INTRODUCTION AND LITERATURE REVIEW

1.1 Background

Fiber composite materials have very high strength and stiffness but low density. This structural efficiency enables these composite materials to be used in a wide variety of applications, especially in aerospace structures. However, advanced composites also have some disadvantages such as poor inter-laminar strength, low damage resistance, low damage tolerance, and poor delamination resistance. Since most of the commonly used advanced composites are made by laying up fibrous reinforcement in a surrounding matrix and the mechanical properties between the plies are dominated by a relatively weak matrix, this weakness causes low damage resistance and low damage tolerance and finally results in low compression-after-impact strength.

A delamination is an interface crack or a debond between two adjacent plies. It is one of the critical failure modes in composite materials. During the manufacture of fiber-reinforced composite laminates, imperfections such as air entrapment or resin starvation may cause initial delamination in the composite. Impact on laminated composites by a foreign body during service may also cause delamination while the surface of the composite structure remains undamaged to visual inspection. This kind of delamination can randomly occur somewhere in the structure. No matter where it occurs it may decrease the overall stiffness and load-carrying capacity of the composite structure. The growth of delamination cracks under the subsequent application of external loads leads to the rapid deterioration of mechanical properties and may cause catastrophic failure of the composite structure. One of the most dominant forms of damage is delamination due to lack of reinforcement in the thickness direction. There are some approaches that can be adopted in order to improve the strength in the thickness direction. Using fully integrated 3D composites such as weaves and braids is one of the methods; however, due to their complexity, limited shapeability, and processability, their applications have been limited. Inserting a pin in the thickness direction can also improve reinforcement in the thickness direction, but currently it is difficult to use this technique in large structures. Another method for providing a reinforcement in the thickness direction is to use stitching through the thickness of the laminate. Only small amounts of out-of-plane reinforcement are needed in order to significantly change the mechanical properties of the structure. A stitched laminate can be formed by using a sewing machine to stitch fiber yarns into a composite preform before curing. Having a stitch in a laminate does not greatly alter the original laminated structure. Further, stitching can be done very fast in automated machines, and is suitable for large structures such as aircraft wings.

Under compression the delaminated part of composite laminate may undergo post-buckling behavior. A delamination may propagate when a foreign body drops on a delaminated composite. Many researchers have studied these subjects by using analytical and numerical methods. Some studies have investigated the effect of stitching on mechanical and impact properties, such as inter-laminar strength and fracture toughness.

A literature review is provided in the next section.

1.2 Literature Review

The literature review is divided into three parts: (a) post-buckling behavior of delaminated composites, (b) impact response of composite structures, and (c) through-the-thickness stitching of composite laminates.

2.1 Research on Post-buckling of Delaminated Composites

In many cases, when delaminated composites are under external compressive loads the delaminated structure will have the capability of carrying loads beyond their buckling loads and may fail in the post-buckling regime. Therefore bifurcation analysis may not be adequate in describing the whole damage process of delaminated composites up to final failure; a post-buckling analysis may be required.

The initial development and growth of delamination in compressed composites are affected by various geometrical parameters, loading conditions, material properties and so on. The different combinations of these parameters can result in different types of buckling and delamination growth behavior. Most studies were based on the static post-buckling solution of homogeneous or laminated plate theory. The energy release rate (G) is considered as the critical parameter and different methods were used to calculate the energy release rate. An assumption that uses Griffith-type fracture criterion with a specific constant critical fracture energy release rate (G_c) was adopted in these studies. When the energy release rate G is greater than critical fracture energy release rate G_c the delamination in the composite may propagate.

Simple analytical and finite element models seem to be popular in analyzing one-dimensional delaminations. Chai et al. [1] used an analytical method to obtain energy release rate by differentiating the strain energy with respect to delamination length. Yin and Wang [2] used the J-integral method to obtain an expression for energy release rate in the post-buckled delaminated plate. Whitcomb [3] adopted the crack closure technique and analyzed the effects of various parameters on energy release rate in a beam-like structure using geometrically nonlinear finite elements.

Sheinman and Soffer [4] investigated the effects of bending-extension coupling and initial imperfection on the post-buckling behavior of a composite beam with various delamination geometries. It was found that the coupling effect significantly reduced the buckling load and increased the post-buckling deformations, and the global post-buckling deformation was shown to be very sensitive to initial imperfections.

Kardomateas and Schmueser [5] proposed a one-dimensional beam-plate model that accounts for the transverse shear effect. Analytical solutions for the critical instability load and the post-buckling deflections were obtained with aid of the perturbation technique. Kardomateas [6] also modeled the post-buckling behavior of a laminate with a thin delaminated sublaminate through a procedure that is based on large deflection theory of the delaminated layer

Chen [7-8] proposed a shear deformation theory and obtained energy release rate by a variational energy principle. He found that the energy release rate is larger with transverse shear effect included for the same applied load. Therefore the initiation of delamination growth will occur at a lower applied load than that evaluated with the classical lamination theory. He also found that the magnitude of the transverse shear effects depends on the delamination location and size.

Davidson and Krafchak [9], Davidson [10], Davidson and Krafchak [11] used crack tip element analysis to determine total energy release rate and individual mode I and II energy release rate in different loading conditions or different delamination cases.

Kyoung and Kim [12] presented an energy method to obtain an analytical solution for determining the buckling load and the growth of delaminated beam-plate structures. In their study the delamination was arbitrary located. They also found that the shear effects decrease the buckling loads and increase energy release rate. The results from their analysis show that the buckling load of a center located delamination is higher than an off-center delamination.

Lee et al. [13] proposed a finite element method based on a layer-wise laminated composite plate theory for solving the post-buckling problem. In their study a contact algorithm, which overcame the physically unallowable overlapping between delaminated surfaces, was used.

There are also several works concerning two dimension post-buckling analysis. Yin and Fei [14] presented an elastic post-buckling analysis of a delaminated circular plate under axis-symmetric compression along its clamped boundary. They found that certain features of the post-buckling behavior are qualitatively similar to the buckling of an axially loaded beam plate containing a one-dimensional delamination. Whitcomb and Shivakumar [15] used virtual crack closure technique to calculate the total energy release rate in a locally post-buckled laminate with embedded delamination. They found that there is a large variation of energy release rate along the delamination front for square and rectangular plates, and delamination growth depends on current delamination aspect ratio, the strain level, and the size of the delamination.

Suemasu [16] investigated an effect of multiple delaminations of composite panels on the buckling loads by using an analytical approach and verified the model using experiments and finite element methods. He pointed out that the buckling load reduces significantly due to the existence of multiple delaminations

Naganarayana and Atluri [17-18] used a multi-plate model, in conjunction with a 3-noded quasi-comforming shell element, to model the delaminated plates. The J-integral technique was used for delamination growth prediction in term of point-wise energy release rate distribution along the delamination edge. The effects of structural parameters such as delamination thickness, size and shape on the post-buckling behavior and on the delamination growth were examined

Shen and Williams [19] studied a post-buckling analysis of laminated plates subjected to combined axial compress and uniform temperature loading. The analysis used a perturbation technique to determine buckling loads and post-buckling behaviors in anti-symmetrically angle-ply and symmetrically cross-ply laminated plates. Klug et al [20] adopted Mindlin plate finite element to perform the post-buckling analysis and to compute energy release rate at the delamination front with aid of the crack closure method in composite laminates which have elliptic delamination shape. The results show that this method is efficient and accurate compared to three-dimensional finite method in calculation of the energy release rate.

1 2 2 Research on Low-Velocity Impact Response and Damage of Delaminated Composite Materials

Low-velocity impact response and damage caused by low-velocity projectile impact has received attention from some researchers When the low-velocity foreign body drops on a structure such as the surface of an airplane wing, it may cause damage such as a delamination which is invisible on the surface and difficult to detect Therefore understanding the low-velocity impact response of a delaminated composite is very important, and a method is needed to predict the damage due to low-velocity impact Graves and Kantz [21] used the maximum shear stress failure criterion to estimate the damage area. Clark [22] provided a model only for qualitative prediction of the delamination size Grady and Sun [23], and Grady and Depaola [24] provided an estimation of the delamination growth due to impact. Choi et al [25] adopted a dynamic finite element method associated with failure analysis to predict threshold of impact of damage and initiation of delamination. Sankar and Hu [26] and Hu [27] used a finite element method to analyze dynamic delamination growth in a composite beam. The delaminated beams were modeled as two offset beams and spring elements were used to connect the beams in the uncracked portion. The dynamic energy release rate was computed from the strain energy in the crack-tip element. Razi and Kobayashi [28] performed finite element analysis and experiments to study damage growth and distribution in cross-ply laminate beams and plates. A quasi-static finite element analysis coupled with a $G_{II} \geq G_{IIc}$ criterion was proposed for the delamination growth, and $G_{II} \leq G_{IIa}$ criterion was used to arrest crack propagation. Sun and Yih [29] investigated the quasi-static characteristics of impact responses and the impact-induced delamination growth of composite laminates subjected to low-velocity impact. They used a spring-mass model to predict contact force history and the peak force was associated with the energy release rate. Thermal loads were included in computing energy release rate. Wang and Vu-Khanh [30] also used the finite element method to model carbon fiber/PEEK cross-ply damaged laminates. They found that a delamination occurred in the form of a Mode II-dominated unstable crack growth and subsequent arrest.

Kwon and Sankar [31-32] performed experiments to study the low-velocity impact damage of quasi-isotropic and cross-ply graphite/epoxy composite laminates. They found that the impact force history and delamination radius could be predicted using the results from a static indentation or flexure test. Sankar [33] reviewed the necessary concepts for understanding low-velocity impact response and damage in fiber composite materials and gave several algorithms for predicting the impact force history to different degrees of approximations. Sankar [33] presented a semi-empirical method for predicting impact damage in composites.

1.2.3 Research Related to Delaminated Composite Materials with Stitches

In transversely stitched composites the delamination is not completely separated but is held together by the stitches. Therefore the propagation of cracks can be prevented in stitched composite materials. Several studies have investigated the effect of stitching on mechanical and impact properties, failure loads, inter-laminar strength, and fracture toughness.

In general there are three types of stitches as shown in Figure 1.1: modified lock stitch, chain stitch, and standard lock stitch. Some parameters of stitches are Stitch density, stitch yarn, and yarn material density. We define the stitch density in a composite laminate by the number of stitches per square inch are reported. This [illegible] [illegible] [illegible] (spacing between two stitch lines). For example, 4X1/4 means a stitch density of 16 where there are 4 stitches per inch and distance between two adjacent stitch rows is 1/4 in. Stitch yarn is the bobbin yarn used in the stitching process. The material density of the stitch yarn is expressed as denier. One denier is the mass in grams of 9000 meters of yarn.

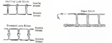

Figure 1.1 Types of lock stitches (Courtesy, Sharma and Sankar [46])

Sawyer [34] used an experimental method to determine the effect of stitching on the static load of bonded composite single lap joint. Up to 38% improvement in static failure load compared with unstitched results was obtained by a single row of stitches near the end of the overlap

Additional row of stitching or different stitch spacing had little effect on static joint failure load.

Su [35] improved the delamination resistance in composite laminates by the use of thermoplastic matrix resin and stitching. There was a 20-30% further improvement of delamination resistance by using stitches. Dexter and Funk [36] conducted an experimental investigation on impact resistance and inter-laminar fracture toughness of stitched quasi-isotropic graphite/epoxy composites. The stitch materials were polyester or Kevlar™ yarns with several parameters. They found that a significant drop in damage areas of stitched laminates compared to unstitched laminates for the same impact energy. The results shown that inter-laminar fracture toughness G_{IC} of stitched laminated with the most effective Kevlar yarn was 30 times higher than unstitched laminates.

Pelstring and Madan [37] proposed a semi-empirical formula to relate a damage tolerance of a composite laminate to stitching parameters. The results showed that Mode I critical energy release rate of a stitched laminate was 15 times higher than an unstitched laminated. Dransfield et al. [38] reviewed the effect of stitching on improving some mechanical properties such as compress-after-impact strength and delamination resistance of composite materials. The advantages and disadvantages of adopting a stitch in a composite structure and the necessary techniques of manufacture were examined. Shu and Mai [39-40] used analytical approaches to investigate the effect of stitching on buckling load and energy release rate of thin film structure. They assumed that the stitches followed a Winkler elastic foundation type of stress-separation relation. The results shown that the strength of composite laminates under edgewise compression can be significantly increased. Jain and Mai [41] proposed two analytical models to study the effect of stitch parameters such as stitch density, stitch thread diameter, and matrix/stitch interfacial shear stress etc. on improving Mode I delamination toughness. They found that a large matrix/stitch interfacial shear stress, high stitch density and a small stitch thread diameter were desirable in order to maximize the delamination growth resistance. Jain and Mai [42] also used an analytical method to study the effect of stitching parameters on Mode II energy release rate in a laminated composite and found that through-thickness stitching can improve Mode II fracture toughness also. Chen and Sun [43] used a finite element method to propose an effective energy release rate for measuring Mode I fracture toughness of a stitched composite laminate. Kang and Lee

14] did an experiment to study the effect of stitching on mechanical and impact properties of woven laminated composites. The mechanical properties were improved at an optimum stitch density compared with unstitched woven laminated composites. The damage area caused by repeated impact was far smaller in stitched woven composites than that in unstitched composites. Wu and Liau [45] also used an experimental method to investigate the behavior of stitched laminates under low velocity impact. They also found that stitching could significantly reduce the delamination area. With increasing the stitch density the damage mechanism changed from delamination in unstitched laminates to the plastic-hinge type of local deformation at the impact location in stitched laminates. Sharma and Sankar [46] performed experiments to study the effects of stitching on CAI (Compression-After-Impact) strength, fracture toughness in Mode I and Mode II. They found that CAI strength, Fracture toughness of Mode I and Mode II can be improved significantly by stitching. Sankar and Sonik [47] used Finite Element and analytical models to study the effect of stitching on Mode II fracture toughness. Dickinson [48] adopted a micro-mechanics approach to characterize the effects of stitching on the elastic constants, in plane strength and inter-laminar mechanical response of undamaged composite laminates. Sankar and Dharmapuri [49] presented an analytical model to simulate delamination growth in laminated DCB (Double Cantilever Beam) specimen with stitches and proposed a simple method to compute the energy release rate due to delamination in the stitched specimen. Jain and Mai [50] studied the effect of reinforced tabs on the Mode I fracture toughness of stitched composites. They indicated that reinforcing aluminum tabs along the length of stitched DCB specimens can alter the failure mechanism of the stitch threads and hence erroneous values for Mode I fracture toughness. Glaessgen et al [51] used finite element method in conjunction with crack closure technique to study the effect of stitching on Mode I and Mode II energy release rate for various debond configurations.

1.3 Objectives and Scope of the Present Study

From the above sections we can realize that one of the most dominant damage in composites is delamination growth due to lack of reinforcement in the thickness direction. Stitching is found to be one of the effective reinforcing methods in the thickness direction of laminated composites. However it is not clearly understood how stitching can delay the delamination propagation of composite laminates subjected to compressive load or a low-velocity impact. The purpose of the present [illegible] is to use analytical and finite element methods to study the effect of stitching on post-buckling and low-velocity impact response of composite structures. In particular the study will focus on the effect of stitching on buckling load, energy release rate, and impact damage resistance.

The organization of this dissertation is as follows. In Chapter 2 an analytical solution for post-buckling of a delaminated composite beam with stitching will be derived. In Chapter 3 a finite element analysis will be given related to post-buckling of a delaminated composite beam with stitching. In Chapter 4 an analytical model for impact response of stitched composite beam is presented. Conclusions drawn from this study and discussions for future research are presented in Chapter 5.

CHAPTER 2

AN ANALYTICAL SOLUTION FOR POST-BUCKLING OF A DELAMINATED COMPOSITE BEAM WITH STITCHING

In this chapter an analytical solution for post-buckling behavior of a delaminated composite beam with stitching is derived based on Rayleigh-Ritz method. The effect of stitching on buckling load and energy release rate is discussed. Non-dimensional parameters for buckling load, energy release rate (G), crack length (a), and stitch stiffness (K) are derived. Although finite element methods can model a stitched composite more realistically, analytical methods have several advantages. Analytical methods provide a closed-form solution to all the desired quantities such as energy release rate, and critical buckling loads. Further, analytical methods allow introduction of nondimensional parameters, and the results expressed in terms of these dimensionless parameters are applicable over a wide range of the actual problem variables such as beam thickness, delamination length, and stitch density.

1 Basic Assumptions

When we model the post-buckling behavior of a delaminated composite beam with stitching the following assumptions are made:

1. A stitch is modeled as a linear cohesive spring. The stiffness of the spring is a function of stitch density, Young's modulus E of the stitch, diameter of the stitch yarn, and thickness of the stitched composite beam. Stitches are smeared averaged on the whole length of the beam, and thus the smeared stitch stiffness should account for the stitch spacing also.
2. A delamination is assumed to be pre-existing before the compressive loading is applied and is located at the center of the beam both in length direction and in thickness direction. Therefore the beam-like structure is symmetric (see Figure 2.1).
3. The deformation shape of the stitched composite beam under post-buckling behavior is assumed to be the same as in an unstitched beam under post-buckling.
4. The laminated beam is approximated as a homogenous beam with an equivalent Young's modulus.

2 Analytical Model

In this section we first derive the buckling load P_{cr} and energy release rate (G) in an unstitched composite beam using the Rayleigh-Ritz method and then obtain the buckling load P_{cr} and energy release rate (G) for a stitched composite beam. A single crack is located at the center of the structure.

2.2.1 Delaminated Composite Beam Without Stitching

A composite beam-like structure without considering through-the-thickness reinforcement is shown in Fig. 2.1

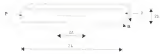

Figure 2 1 A delaminated beam

The length of the beam is $2L$, B is the width, $2h$ is the thickness of the beam, $2a$ is the delamination length and P is the compressive load.

The delaminated composite beam is composed of two parts. One part is the uncracked portion and the other is the cracked portion. The cracked portion is modeled as two sub-laminated beams, called top sub-laminated and bottom sub-laminate. When the compressive load P reaches the buckling load P_{cr}, the cracked portion of the beam-like structure will deform. Therefore let us consider the deformation of the delaminated portion first. After the compressive load P exceeds the buckling load P_{cr}, the cracked portion of the beam will deform as shown in Figure 2.2.

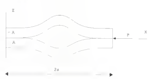

Figure 2.2 Deformed shape of sub-laminates

The Strain energy density of cracked portion is

$$U_c = 2\left(\int_A \frac{1}{2} E\varepsilon_x^2 \, dA\right) \tag{2.1}$$

here

$$\varepsilon = \frac{\partial u}{\partial x} + \frac{1}{2}\left(\frac{dw}{dx}\right)^2$$

$$= \frac{\partial\left(u_0 - z\frac{dw}{dx}\right)}{\partial x} + \frac{1}{2}\left(\frac{dw}{dx}\right)^2 \qquad (2.2)$$

Here u is [illegible] displacement in the x direction, w is the displacement of top sublamated beam in the [illegible] direction. ε is the [illegible] strain of top sublaminated beam in x direction. The cross-sectional area of the sublaminates is represented by A and E is the Young's modulus. Assume the forms of u and w as $u=cx$, $w=d\sin \pi x/2a$, where c and d are unknown coefficients to be determined.

The strain energy of the delaminated portion of the beam can be derived as

$$U = \int_0^{a} U_1\, dx$$

$$= EA\left\{\frac{c\pi^2 d^2}{4a} + c^2(2a)\right.$$

$$\left. + \frac{3\pi^2 d^4}{32(2a)^3} + \frac{2EI\pi^4 d^2}{(2a)^3}\right\} \qquad (2.3)$$

where I is the moment of inertia of each sublaminate.

The potential energy V of the external loads is given by

$$V = (-P)c(2a) \tag{2.4}$$

Total energy Π

$$\Pi = U + V \tag{2.5}$$

Using the Rayleigh-Ritz method

$$\frac{\partial \Pi}{\partial c} = 0 \tag{2.6}$$

$$\frac{\partial \Pi}{\partial d} = 0 \tag{2.7}$$

Substituting for the energy terms U and V we can obtain the following two equations

$$EA\left\{\frac{\pi^2 d^2}{4a} + 2c(2a)\right\} + P(2a) = 0 \tag{2.8}$$

$$EA\left\{\frac{\pi^2 c}{2a} + \frac{3\pi^4 d^2}{8(2a)^3}\right\} + \frac{4EI\pi^4}{(2a)^3} = 0 \tag{2.9}$$

It may be noted that the above equations are nonlinear and lead to multiple solutions. Solving these two equations we obtain the coefficients c and d as follows.

One possible solution set is:

$$c = -\frac{P}{2AE} \tag{2.10}$$

$$d = 0 \tag{2.11}$$

This solution describes the behavior of the cracked portion of the beam where the compressive load is less than the buckling load P_{cr}. Since $d=0$, there is no deformation in z direction. The relation between compressive load P and axial displacement u_0 takes a simple form:

$$u_0 = -\frac{Px}{2EA} \tag{2.12}$$

The end shortening δ_c at $x=2a$ is given by:

$$\delta_c = -u_0 \,|_{x=2a} = \frac{Pa}{EA} \tag{2.13}$$

The other possible solution set is:

$$c = -\frac{3P}{2AE} + \frac{8\pi^2 I}{A(2a)^2} \tag{2.14}$$

$$d^2 = \frac{4P(2a)^2}{EA\pi^2} - \frac{32I}{A} \tag{2.15}$$

In order for $d^2 > 0$, we have

$$P > P_{cr} = \frac{8\pi^2 EI}{(2a)^2} \tag{2.16}$$

here P_{cr} is the critical buckling load.

This solution set describes the behavior of the cracked portion of the beam where the compressive load is greater than the buckling load P_{cr}. There is a deformation in the z direction. The relation among compressive load P and axial displacement u_0 and deformation shape w are:

$$u_0 = -\frac{3Px}{2AE} + \frac{8\pi^2 Ix}{A(2a)^2} \tag{2.17}$$

$$w = d\sin^2\frac{\pi x}{2a} \tag{2.18}$$

here d is obtained from Equation 2.15 for a given P. End-shortening δ_c at x=2a can be expressed as shown as:

$$\delta_c = -u_0\big|_{x=2a} = \left(\frac{3P}{2AE} - \frac{8\pi^2 I}{A(2a)^2}\right)(2a) \tag{2.19}$$

Based on Equation 2 13 and 2 19 the relation between the compressive load P and the end shortening δ_c will be as shown in Figure 2 3.

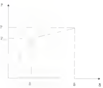

Figure 2 3 The relation between compressive load P and end shortening δ_c

In Figure 2.3 δ_{cr} is end shortening at critical buckling load P_{cr} and δ is end shortening at an arbitrary compressive load P.

Based on Figure 2.3, the strain energy U_l of the buckled portion can be written as:

$$U_1 = \frac{1}{2}P_{cr}\delta_{cr} + \frac{1}{2}(P_1 - P_{cr})(\delta_{c1} - \delta_{cr})$$

$$= \frac{3P_1^2 a}{2EA} - \frac{4\pi^4 EI^2}{Aa^3} \qquad (2\ 20)$$

We can extend the results to the entire composite beam. After the compressive loads P reaches the buckling load P_{cr}, the beam-like structure will deform as shown in Figure 2.4.

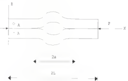

Figure 2.4 Deformed shape of the entire delaminated beam

The relation between the compressive load (P) and end-shortening (δ) is

$$P = \frac{EA\delta}{l} \qquad (P < P_{cr}) \qquad (2.21)$$

$$P = \frac{AE}{2a+L}(\delta + \frac{4I\pi^2}{Aa}) \qquad (P > P_{cr}) \qquad (2.22)$$

The strain energy U of the entire beam is the sum of strain energy U_1 in the cracked portion of the beam and strain energy U_2 in the uncracked portion of the beam, and it has the following form

$$U = U_1 + U_2$$

$$= \left(\frac{3P^2 a}{2EA} - \frac{4EI^2 \pi^4}{Aa^3} \right) + \frac{P^2 (L - a)}{2EA} \tag{2.23}$$

Strain energy release rate (G) at the crack tip is obtained by differentiating total strain energy U with respect to half of crack length a [53]. Then the expression for G can be derived as

$$G = \frac{1}{2B} \frac{\partial U}{\partial a}\bigg|_{\delta}$$

$$= \frac{1}{2B} \left\{ \frac{4AE\delta^2}{(4a + 2L)^2} + \frac{8EI\pi^2 \delta (8a + 2L)}{(4a + 2aL)^2} \right.$$

$$\left. + \frac{16EI^2 \pi^4 (12a^2 + 4aL)}{A(4a^3 + 2a^2 L)^2} - \frac{12EI^2 \pi^4}{Aa^4} \right\} \tag{2.24}$$

2.2.2 Delaminated Beam with Through the-Thickness Stitches

A delaminated beam with stitching is depicted in Figure 2.5.

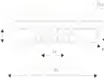

Figure 2.5 A stitched delaminated beam

Now let us consider the delaminated portion of the beam with stitching. We assume that the buckled shape of the sublaminates is similar to that without stitches as described in the previous section. Thus we assume $u_0=cx$ and $w=d\sin^2\pi x/2a$ where unknown coefficients c and d will be different for the unstitched case. The deformed shape of the cracked portion is depicted in Figure 2.6

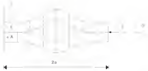

Figure 2 6 Deformed shape of crack portion with stitching

Strain energy U of the delamated portion of the beam with stitching includes two parts: strain energy $U_{nostitch}$ from the delaminated portion of the beam without stitching and the energy U_{stitch} contributed by the stitches. The total strain energy U is of the following form:

$$U = U_{nostitch} + U_{stitch}$$

$$= U_{nostitch} + \int_{0}^{2a} \frac{1}{2} K (2w)^2 \, dx \qquad (2\ 25)$$

where K is foundation constant that represents the stiffness of the sheared stitches. The foundation constant K is related to the actual stitch parameters as

$$K = \left(\frac{A_s E_s}{2h}\right) NB \tag{2.26}$$

where A_s is the area of cross section of a stitch (2 bobbin yarns), E_s is Young's modulus of stitch material (bobbin yarn); $2h$ is the total of thickness of uncracked beam, N is the stitch density (number of stitches/unit area), and B is the width of the beam in the y-direction.

After using a procedure similar to that for an unstitched beam, we derive the buckling load P_{cr} of a delaminated beam with stitches as follows:

$$P_{cr} = \frac{8EI\pi^2}{(2a)^2} + \frac{3K(2a)^2}{\pi^2} \tag{2.27}$$

From Equation 2.27 we can see that the first part of P_{cr} is the same as the buckling load of an unstitched beam, and the second part of the equation is contributed by the stitches. Therefore stitching indeed can improve the buckling load.

Now we can extend the result to the entire stitched beam. The deformation of the beam undergoing post-buckling is shown in Figure 2.7.

The relation between compressive loads P and end ortening δ is

$$P = \frac{AE}{L}\delta \qquad (P < P_{cr}) \tag{2.28}$$

$$P = \frac{AE}{2a+L}\left(\delta + \frac{4I\pi^2}{Aa} + \frac{24Ka^3}{EA\pi^2}\right) \qquad (P > P_{cr}) \tag{2.29}$$

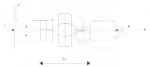

Figure 2.7 Deformed shape of the delaminated beam with stitches

When compressive loads P is greater than the buckling load P_{cr} of the stitched beam total strain energy U of the antire delaminated beam with stitching is:

$$U = \frac{P^2(L-a)}{2EA} + \frac{3P^2a}{2EA} - \frac{a}{EA}\left(\frac{2EI\pi^2}{a^2} + \frac{12Ka^2}{\pi^2}\right)^2 \tag{2.30}$$

Strain energy release rate G (when P

$$G = -\frac{1}{2B}\frac{\partial U}{\partial a}\bigg|_{\delta}$$

$$G_{stitch} = \frac{1}{2B}\left\{\frac{576K^2(20a^6+12a^5L)}{(4a+2L)^2EA\pi^4} + \frac{192KI(4a^2+4aL)}{A(4a+2L)^2}\right.$$

$$\left. + \frac{48K\delta(8a^3+6a^2L)}{\pi^2(4a+2L)^2} - \frac{48KI}{A} - \frac{720K^2a^4}{EA\pi^4}\right\} \tag{2.31}$$

Let us define the nondimensional parameters as $P_{cr}' = P_{cr}/EA$, $G' = G/Eh$, $a' = a/L$, $B' = B/L$, $h' = h/L$, $\delta' = \delta/L$, $K' = K/E$. P_{cr}' is non-dimensional buckling load; G' is the nondimensional energy release rate, a' is the nondimensional half crack length of the structure; B' is the ratio of the width of the structure to the half length of the beam, h' is the ratio of the thickness to the length of the structure; δ' is the nondimensional end shortening of the beam along the axial direction, K' is the nondimensional stiffness of the stitches. After tedious algebraic manipulations we can derive the following relations

$$P_{cr}' = \frac{\pi^2 h'^2}{6a'^2} + \frac{12K'a'^2}{\pi^2 B'h'} \tag{2.32}$$

$$\iota_r = \frac{2\delta^2}{(4a+2)^2} + \frac{\pi^4 h^4 (6a^2+2a)}{9(4a^3+2a^2)^2} - \frac{288K^2(20a^4+12a^3)}{\pi^4 B^2 h^2 (4a+2)^2}$$

$$+ \frac{\pi^2 h^2 \delta (8a+2)}{3(4a^2+2a)^2} - \frac{8K h (4a^2+4a)}{B(4a+2)^2} + \frac{2K h}{B}$$

$$- \frac{24K\delta(8a^3+6a^2)}{\pi^2 B h (4a+2)^2} - \frac{\pi^4 h^4}{24a^4} + \frac{360K^2 a^4}{\pi^4 B^2 h^2} \qquad (2.33)$$

In the following section the results of the analytical model are discussed in term of the nondimensional parameters.

2.3 Results and Discussion

The results presented in this section are based on Equation 2.32 and 2.33. In all numerical examples h'=0.02 and δ'=0.08

Figure 2.8 shows the variation of buckling load P_{cr}' as a function of semi-crack length a' for various values of stitch parameter K'. From Figure 2.8 we can observe that the non dimensional buckling loads P_{cr}' is not affected by stitching when the range of the nondimensional crack length a' is from 0.05 to 0.1. When a' is greater than 0.1, P_{cr}' for of unstitched beam decreases as the nondimensional crack length a' increases. This is understandable because a [illegible] buckles more easily with increasing crack length. When we look at stitched beams in the range $0.1<a'<0.4$ (see Fig. 2.9) the buckling load is always higher than that of unstitched beam, and further the buckling load P_{cr} increases as the stiffness of stitching K' increases. In a stitched beam an interesting phenomenon occurs, the buckling load P_{cr}' decreases as the crack length a' increases in the range $0.1<a'<0.2$, however for $0.2<a'<0.4$ the buckling load P_{cr} does not decrease due to increasing crack length a', but in contrast P_{cr} increases to some extent depending on the stiffness of stitching. The reason is that the longer crack, the more stitches involved in the structure and the stitches hold the structure together more tightly, therefore the buckling load P_{cr}' can be improved in the stitched beam even with longer delamination. A similar behavior was obtained by Shu and Mai [38] for the case of thin film delamination with stitches. Figure 2.9 shows this phenomenon in detail.

In Figure 2.10 the relation between nondimensional energy release rate G' and nondimensional crack length a' and the effect of K' on energy release rate G' for a [illegible] ing δ=0.1 and [illegible]. When crack length a' is less than 0.1 the stitching has no effect on non-dimensional energy release rate G'. As the nondimensional delamination size a' grows beyond 0.1 the effect of stitching becomes significant. The energy release rate G decreases in a stitched beam compared to that in an unstitched beam. The larger the stiffness of the stitching, smaller is the nondimensional energy release rate in stitched beams. Therefore using a stitching can decrease the energy release rate at the crack tip, and the crack propagation can be delayed. The crack will propagate when the energy release rate is greater than the critical energy release rate (fracture toughness G_c). The variations of G' have similar tendency in both stitched beam and unstitched beam. Nondimensional energy release rate G' dramatically increases with crack length for smaller delaminations, and reaches maximum G_{max} at certain crack length a' and then G' goes down as the delamination size increases. Whether a crack will propagate or not depends on fracture toughness G_c. Whether it will be a stable crack propagation or an unstable propagation depends on the rate of change of energy release rate G with delamination size a. Referring to Figure 2.10, we can note that in the beginning the crack [illegible] dG'/da' is negative and hence the crack propagation will be stable

In Figure 2.11 the relation between nondimensional energy release rate G' and nondimensional stitch stiffness at a given crack length ($a'=0.2$) is examined and the effect of non-dimensional end shortening δ' is shown. It demonstrates that energy release rate G' decreases with increasing the stiffness K' of stitching. The more non-dimensional end shortening δ' is, the more nondimensional energy release rate G' has

The variation of G' with δ' for various stitch stiffnesses is shown in Figure 2.12. The results correspond to $a'=0.2$. The relations were very similar for other crack lengths also. From Figure 2.12 one may note that the G' remains close to zero in the beginning, but increases after certain critical δ'. The variation of G is approximately quadratic in δ'. Further, it may be noted that for a given δ', G' decreases with the K'. This is brought out clearly in Figure 2.12, where G is plotted as a function of K' for various δ'. One can see that the dramatic decrease in G' with increasing K'

In summary stitching always increases the critical load for buckling in delaminated beams It reduces the energy release rate at the crack-tip thus preventing or delaying the onset of delamination propagation Both these effects are very much dependent on the stitch parameter K' which is given by (see Equation 2 26):

$$K' = \frac{A_s E_s}{2h} \frac{NB}{E} \qquad (2\ 34)$$

From Equation 2 34 one can see that K' is proportional to the stitch axial stiffness and stitching density, but inversely proportional to the equivalent Young's modulus of the parent laminate. Thus one needs to use high density, high stiffness stitches for stiffer laminates.

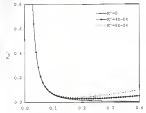

Figure 2.8 Variation of P_{cr}' with a' for different K' in the range $0<a'<0.4$

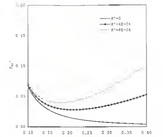

Figure 2.9 Variation of P_{cr}' with a'
for different K'
in the range $0.1<a'<0.4$

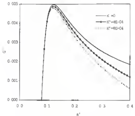

Figure 2.10 Variation of G' with a' for a given (δ'=0.1)

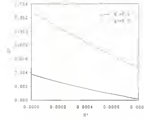

Figure 2.11 Variation of G' with K' for a given a' (a'=0.2)

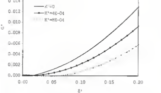

Figure 2 12 Variation of G with δ for a given a (a =0.2)

CHAPTER 3
FINITE ELEMENT ANALYSIS OF A DELAMINATED COMPOSITE WITH STITCHING

As discussed in Chapter 2 delaminations can greatly reduce the compressive load carrying capacity of laminated composite structures Through-the-thickness stitching seems to be helpful in increasing the critical load at which a delaminated beam becomes unstable under compressive loading In Chapter 2 an analytical solution for post-buckling of a stitched composite with a delamination was given. Several assumptions were made in order to obtain a closed form solution. In this chapter finite element analysis is used to investigate the effect of stitching on the post-buckling behavior of a stitched composite. Although analytical models provide insight into the effects of stitching, more detailed behavior of a structure can be obtained using finite element models Several restrictions of the analytical approach can be easily removed in FE models. For example, the analytical model assumes the beam is homogeneous and orthotropic, whereas FE models can handle laminated composites. Unlike in the analytical [illegible] the FE model [illegible] parameters, [illegible] material properties, [illegible] and the energy [illegible] under axial compression.

3.1 Specimen

The specimen considered for finite element analysis is made up of 48 unidirectional AS4 graphite/epoxy plies. The material properties for each lamina are $E_1=19.4\times10^6$ psi, $E=1.3\times10^6$ psi, $G_{LT}=0.7\times10^6$ psi, $\nu=0.28$. The length L of the specimen is 5 inches (127mm). The width B is 1 inch (25.4mm) and the thickness H is 0.27 inch (6.86mm). A single delamination (length of 2a) is located at a distance h from the top surface of the beam. The specimen is depicted in Figure 3.1. The specimen is under axial compression. The FE analysis is used to simulate the compression test. In particular we are interested in the load-end shortening relationship and energy release rate as a function of the load.

Three stitch yarn materials were considered Glass 1 (3570 denier), Kevlar (1600 denier) and Glass 2 (5952 denier) bobbin yarn The stitch densities are 4X1/4" and 8X1/8". For example 4X1/4" stitching pattern means a number of 16 stitches per square inch where the pitch is 1/4 inch and the distance between two adjacent stitch lines is 1/4 inch

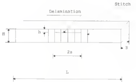

Figure 3 1 A delaminated beam-like structure with stitche

3.2 Finite Element Model

The commercial finite element software ABAQUS [54] was used to simulate the stitched composite with through the width delamination This specimen is modeled by two [illegible] top beam and bottom beam The nodes of each beam are distributed uniformly along the axial direction Type B21 element, which considers transverse shear effect is adopted The stiffness matrix of this type is given in ABAQUS Theory Manual [55] The element size is chosen as 0.0125 inch. In an undelaminated portion the connection between top and bottoms is achieved by using the EQUATION command. The boundary conditions that were implemented are depicted in Figure 3.2.

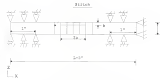

Figure 3 2 Boundary condition in a delaminated beam with through-the-thickness stitches

The relations between the top and bottom beam displacements for the uncracked portion of the composite are as follows

$$u_t - u_b = \frac{h_t}{2}\psi_t + \frac{h_b}{2}\psi_b \qquad (3\ 1)$$

$$w_t - w_b = 0 \qquad (3\ 2)$$

$$\psi_t = \psi_b \qquad (3\ 3)$$

In the above three equations *t* and *b* denote the top and bottom beam respectively, *u* is the nodal displacement in the x direction, *w* is the nodal displacement in the z direction and *ψ* is the rotation.

Through-the-thickness stitches are modeled as linear springs using SPRING2 elements in ABAQUS Two spring elements are used to model each stitch One spring represents the resistance offered by the stitch to relative transverse displacements of the top and bottom beams The second spring element represents the relative displacement in the axial (longitudinal) direction. These spring elements connect the two corresponding nodes on the top and bottom beams. The relative displacement across a SPRING2 element is the difference between the ith component of displacement of the spring's first node and the ith component of displacement of the spring's second node If we denote the axial and transverse displacements by u and w, the relative displacements are (see Figure 3 3):

$$\Delta u = u_2 - u_1 \qquad \Delta w = w_1 - w_2 \tag{3 4}$$

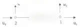

Figure 3 3 Node specification for SPRING2 element

The procedure for determining the spring constants of the stitches is as follows Figure 3 4 shows a stitch where the beam surfaces have relative displacements in both x and z directions. The initial length of the stitch is the total thickness of the beam, H The relative displacements in the x and z directions are Δu and Δw, respectively. The elongation of the stitch ΔL is related to the displacement components by

$$\Delta u = \Delta L \cos\theta$$

$$\Delta w = \Delta L \sin\theta \tag{3 5}$$

here θ is the [illegible] 3 4). The tensile force in the stitch is given by

$$F = \frac{A_s E_s}{H} \Delta L \tag{3 6}$$

here A_s and E_s are the area of cross section and Young's modulus of the stitch yarn. It should be remembered that there are two yarns in each stitch (see Figure [illegible]). The x and z components of the force F are Fx $F\cos\theta$ and Fz-$F\sin\theta$ Substituting for F from Eq 3 6 we obtain

$$F_x = \frac{A_s E_s}{H} \Delta L \cos\theta = \frac{A_s E_s}{H} \Delta u$$

$$F_z = \frac{A_s E_s}{H} \Delta L \sin\theta = \frac{A_s E_s}{H} \Delta w \tag{3 7}$$

From Equation 3-7 it may be seen that the stiffness of the spring in the FE model should be equal to $A_s E_s / H$ In fact the stiffness of both the springs, horizontal as well as vertical, happens to be the same

3 3 Post-Buckling Analysis

The post-buckling analysis requires that an initial imperfection be specified for the beam Usually the imperfection shape is a certain linear combination of several buckling mode shapes. Thus a linear bifurcation analysis has to be performed to determine the buckling mode shapes. In the present analysis only the first mode shape was considered in the initial imperfection. The imperfection amplitude was 5% of the eigenmode calculated by ABAQUS.

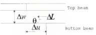

Figure 3.4 Stitch deformation

The nonlinear analysis used the Riks algorithm in order to determine the successive equilibrium positions. To analyze a post-buckling problem, it must be turned into a problem with continuous response instead of bifurcation. This effect can be accomplished by introducing an initial imperfection into a "perfect" geometry so that there is some response in the buckling mode before the critical load is reached. The post-buckling problem is a geometrically nonlinear static problem. Static equilibrium states during the unstable phase of the response can be found by using the modified Riks method. This method is used for the case where the load magnitudes are governed by a single scale parameter. The method can provide solutions even in the case of complex, unstable response. The Riks method uses the load magnitude as an additional unknown; it solves simultaneously for load and displacements. Therefore, another quantity must be used to measure the progress of the solution. ABAQUS uses the arc length, l, along the static equilibrium path in load-displacement space. This approach provides solutions regardless of whether the response is stable or unstable. The modified Riks algorithm is described in detail in [55].

3.4 Energy Release Rate

The purpose of stitching or any other forms of through-the-thickness reinforcement is to increase the buckling load and also to prevent the cracks from propagating further. Energy release rate at the crack tip has been found to be a useful parameter in predicting crack propagation in laminated composites. The delamination is expected to propagate further when the energy release rate exceeds the corresponding fracture toughness value of the composite material system. Delaminations have a higher [illegible] the propagation along the plane of delamination as interlaminar fracture toughness is much lower for most laminated composites. In particular Mode I (opening mode) interlaminar fracture toughness is about one-half of Mode II (shearing mode) fracture toughness. For example, the values for a typical AS4/3501-6 graphite/epoxy composite are [46]: G_{Ic} = 300 N/m and G_{IIc} = 670 N/m. Thus the effectiveness of stitching can be judged by the reduction in energy release rate, G, at the crack tip.

There are three different methods to compute G: (i) computing stress intensity factor at the crack-tip, (ii) Strain Energy Density Method, (iii) Virtual crack growth method. The first method requires detailed three-dimensional stress field near the crack tip, which can only be obtained by using three-dimensional finite elements with a fine mesh. Since we are using structural elements in the present analysis, the stress intensity factor approach cannot be used. The strain energy density method developed by Sankar [52] requires computation of energy densities just behind and ahead of the crack tip. However in the case of stitched composites, the stitch forces affect the energy densities significantly, and hence a very fine mesh is needed near the crack tip. Further ABAQUS does not provide the energy density values readily, and they need to be computed from the force and moment resultant just ahead and behind the crack tip. Hence the third method is used in the present study, and it is explained below

Energy released rate G is computed by using the following formula [53]

$$G = -\frac{1}{2B}\frac{\partial U}{\partial a} \tag{3.8}$$

here U is the strain energy in the beam for a given displacement, a is the crack length, and B is the width of the beam. In this method the load-end shortening relation P-δ is developed using the aforementioned nonlinear FE analysis. For a given displacement (end shortening) the area under the P-δ diagram up to the displacement represents the strain energy stored in the beam. Let it be equal to $U(\delta)$. The change in strain energy is computed numerically by repeating the nonlinear FE analysis for a crack length $a+\Delta a$, where Δa is the incremental crack length. The area under the new P-δ curve represents the strain energy for the new crack length. Then G is obtained by numerically differentiating $U(\delta)$ (see Fig. 3.5)

$$G = -\frac{1}{2B}\frac{\Delta U}{\Delta a}$$

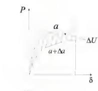

Figure 3.5 Strain energy change due to crack growth

3.5 Results and Discussion

In this section the results of the nonlinear FE analysis are presented. The effects of stitching are understood by analyzing the load-end shortening diagrams, P-δ curves, for various types of stitches. The second quantity of interest is the energy release rate G at the crack tip. The G is also plotted as a function of δ for various stitches. Another important and interesting information is the amount of axial strain in the stitches, especially during the post-buckling process. Although stitches prevent delamination propagation by reducing the G, they are subjected to strain by the beam segments that tend to buckle. Thus the strains in the stitches are also plotted as a function of δ

Three types of stitch yarns were used in the numerical example. Kevlar (1600 denier), Glass 1 (3570 denier), and Glass 2 (5952 denier). Their properties are listed in Table 3.1. Two types of stitch patterns were considered: 4x1/4" (16 stitches per square inch) and 8x1/8"(64 stitches per square inch). The properties of the graphite/epoxy and the specimen dimensions were described in section 3.1. The delamination was assumed to be at a distance equal to 1/4th of the total thickness from the top surface of the beam, i.e., h=H/4

Table 3.1 Stitch parameters

STITCH YARN	LINEAR DENSITY IN DENIERS (gm/9,000m)	MASS DENSITY ρ (gm/cm^3)	AREA OF CROSS SECTION A_S (cm^2)	YOUNG'S MODULUS E_S (GPA)	AXIAL RIGIDITY A_SE_S (N)
Kevler	1600	1.50	0.1185×10^{-2}	130	15.405×10^3
Glass 1	3570	2.49	0.1593×10^{-2}	85.5	13.620×10^3
Glass 2	5952	2.49	0.2656×10^{-2}	85.5	22.709×10^3

The P-δ diagrams [illegible] and 64 ssi are given in Figures 3.6 and 3.7, respectively. It is clearly seen [illegible] by 20-30% depending on the stitch material and stitch density. It is also seen that the difference in maximum [illegible] due to different stitch materials is not significant. The effects of stitch density on the maximum load can be inferred from Figure 3.8. It may be seen that there is a slight increase in the maximum load due to an increase in stitch density from 16 ssi to 64 ssi. The results presented in Figure 3.6 through 3.8 are for a crack length of 1 inch.

Figure 3.9 shows the effects of various stitches on the maximum load as a function of the crack length. It should be noted that the beam length is 5 inches, however the effective length is only 3 inches (see Figure 3.2). From Figure 3.9 it is seen that stitching has no effect for very short delaminations (a<1 in). For 0.5 in. < a < 1.5 in. the 64 ssi specimens carry almost the same maximum load as the undelaminated specimens. That is, the high density stitching is able to completely suppress delamination buckling and restore the original load carrying capacity. The 16 ssi specimens also show marked improvement in the maximum load. However for a>2.0 inches the effect of stitching seems to diminish. This is because the delamination length approaches the total length of the beam, and global buckling takes over the sub-delamination buckling. During global buckling the delamination is under more shearing mode than opening mode, and the stitches are not that effective in suppressing the relative sliding motion of the delaminated surfaces.

The effects of stitching on energy release rate G are shown in Figure 3.10 through 3.12. Figure 3.10 corresponds to a stitch density of 16 ssi. It is seen that G is almost negligible until the sublaminate buckling begins. Thereafter the G rises rapidly with the end shortening of the beam. The stitches are able to delay the point when G begins to rise. For example, in Figure 3.10, G begins to rise at $\delta=0.03$ in. in an unstitched beam, whereas it is delayed until $\delta=0.55$ in. in stitched beams. Further, the G is greatly reduced compared to the unstitched beam. For $\delta=0.1$ in. the value of G is reduced from about 800 lb./in. in an unstitched beam to about 100 - 200 lb./in. in stitched beams. Further it can be seen that stitches with higher axial rigidity (see Table 3.1) cause the greatest reduction in G.

Similar results for 64 ssi stitching are presented in Figure 3.11. Both stitch densities are compared with unstitched beam in Figure 3.14. It may be seen that 64 spi stitching offers slightly higher reduction in G

As mentioned earlier monitoring the strains in the stitches is an important consideration in analyzing stitched specimens. Because stitch yarns could break if the strains exceed the allowable limit and this could trigger a domino effect of successive stitch failures and dynamic delamination propagation, and lead to catastrophic failure. The strains in various stitches as a function of end shortening are shown in Figure 3.13. It should be noted that the crack length is 1 inch and the stitch pattern is 4x1/4". Stitch 3 (Figure 3.13) is at the center of the beam and thus undergoes large strains. Stitch 1 is actually at the crack tip and hence there is no strain at all. Stitch 2 is in between stitches 1 and 3. The variation of stitch strain with end shortening is strikingly similar to that of G discussed earlier.

The strains of stitches located at the center of beam in various stitch materials and stitch patters are shown in Figure 3.14. It may be seen that the strains are sensitive to the stitch material as well as the stitch density. In general the strains are significantly less for higher stitch density. Further, stitches with lower axial stiffness (A_sE_s) undergo larger strains.

From the above discussion we can arrive at the following conclusions:

1. Stitching can improve the buckling loads of delaminated beams. The increase is not sensitive to the three types of yarns used in this study. The yarns had axial rigidities in the range of 13,000 N - 223,000 N and they seem to perform equally well. However, the maximum load increases with the stitch density. This is consistent with the experimental observation of Sharma and Sankar [46].
2. Through-the-thickness stitches significantly reduce the energy release rate at the crack tip. They also increase the end shortening required to cause sublaminate buckling when the energy release rate rises rapidly. By reducing the energy release rate stitching prevents the crack propagation which may lead to catastrophic failure of the specimen. The axial rigidity of the stitches also affects the energy release rate. The Higher axial rigidity the greater is the reduction in G.
3. The maximum strain in the stitches depends strongly on the axial rigidity of the stitches and the stitch pattern. The stitches with small axial

[illegible] undergo large axial strains during [illegible] e buckling.

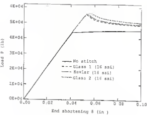

Figure 3.6 Compressive load vs. end shortening at crack length (a=1 in.)

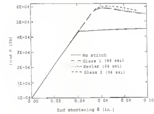

Figure 3.7 Compressive load vs. end shortening at crack length (a=1 in.)

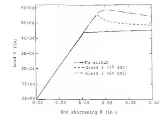

Figure 3.8 Compressive load vs. end shortening at crack length (a=1 in.)

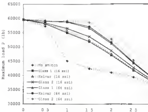

Figure 3.9 Maximum load vs. crack length

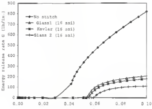

Figure 3.10 Energy release rate vs. end shortening (a=1" h/H=1/4)

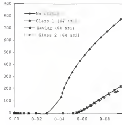

Figure 3 11 Energy release rate vs end shortening (a=1" h/H=1/4)

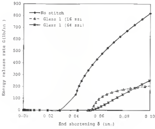

Figure 3.12 Energy release rate vs end shortening (a=1" h/H=1/4)

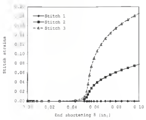

Figure 3.13 Stitch strains vs end shortening
(a=1" h/H=1/4)
Stitch: Glass 1 (16 ssi)

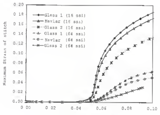

Figure 3.14 Maximum strain in a stitch vs. end shortening (a=1" h/H=1/4)

CHAPTER 4
EFFECT OF STITCHING ON LOW-VELOCITY IMPACT RESPONSE

In the previous two chapters we noted that a delaminated beam is susceptible to buckling failure under axial compression and that stitching can greatly improve its compressive load carrying capacity. During sublaminate buckling the stitches are predominantly under tension, and the fracture mode is close to Mode I or the opening mode. Another type of loading that can be detrimental to delaminated beam is low-velocity foreign object impact. Composite structures are prone to low velocity impact damage due to dropped hand tools, runway debris, hail stones etc. If the composite structure has prior delaminations, then the impact force can cause them to propagate, leading to catastrophic failure. Translaminar reinforcements such as stitching are expected to prevent delamination propagation during foreign object impact.

In this chapter we study the effects of stitching on the impact response of delaminated beams. Several assumptions are made to simplify the problem so that the focus can be on the effects of various stitching parameters

The impact problem is illustrated in Figure 4.1. The force acting on the beam is not known a priori, and has to be calculated as part of the solution of the problem. A major difference between the impact loading and the compressive loading discussed in the earlier chapters is that the delamination is under pure Mode II (shearing mode) conditions. Previous experimental studies by Sharma and Sankar [46] have found that under pure Mode II the stitches try to plough through the matrix, and the resistance offered by the matrix is responsible for the increase in apparent fracture toughness. Thus the stitch model has to be modified to account for this phenomenon.

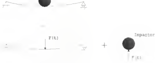

M_0: Impactor mass

V_0: Impact velocity

t Time Variable

Figure 4.1 A structure under impact

In the following sections we discuss the assumptions made in simplifying the impact problem, the stitch model and the impact simulation procedure. The results focus on the extent of delamination propagation due to impact in specimens with different stitch densities.

4.1 Basic Assumptions

The following assumptions are made to simplify the impact simulation:

1. The velocity of impact is low compared to the velocities of wave propagation in the composite beam.
2. The projectile is assumed to be rigid compared to the target. Therefore the impactor can be treated as a rigid body and its equation of motion is greatly simplified.
3. The target, laminated beam in the present case, is highly flexible. The deflection of the beam is expected to be much higher than the local indentation, and hence the Hertzian indentation effects can be neglected.
4. The impactor mass is much greater that that of the beam, and hence the impact duration will be very long compared to the fundamental period of vibration of the beam. Therefore the target can be represented

by a single spring mass system. The stiffness of the spring can be approximated by the static beam stiffness *k* at the impact location.

5 An embedded central delamination is assumed to be pre-existing in the laminated beam. The delamination is symmetrically located in the simply supported beam.

Because of Assumption 4 above we need to compute only the static stiffness of the delaminated beam due to a central transverse force. We will assume that the delamination will propagate along the same plane when the G exceeds G_{IIc} Mode II fracture toughness of the parent laminate.

The resistance offered by the matrix under shearing mode is computed as follows. The ploughing resistance of the stitches can be represented as a distributed shear traction (force/unit length) at the interface of the two sublaminates that are stitched together. The traction p_0 is estimated as:

$$p_0 = \frac{B}{s}\frac{Dh\sigma_y}{n}$$

here B is the beam width, D is the diameter of stitch yarn, h is the greater of the two sublaminate thicknesses, σ_y is the yield stress of the surrounding matrix, s is the stitch spacing in the width direction, and n is the number of stitches per inch. In terms of stitch density the distributed traction can be written as:

$$p_0 = NBDh\sigma_y$$

where N=1/(nxs) is the number of stitches per unit area. As the delamination propagates new stitches come into action in the freshly created delamination areas, and they offer additional shear resistance. This assumption is consistent with the experimental observations of Sharma and Sankar [46]

4.2 Analytical Model

The equation of motion of the impactor along with the initial conditions can be written as:

$$M_0 \frac{d^2 q}{dt^2} = F(q) \qquad (4.1-a)$$

$$q(0) = 0 \qquad (4.1-b)$$

$$\frac{dq}{dt}\Big|_{t=0} = V_0 \qquad (4.1-c)$$

where M_0 is the impactor mass, q is the impactor displacement which is same as the transverse deflection of the target beam at the point of impact, V_0 is the initial velocity of the impactor or the impact velocity, and $F(q)$ is the contact force. The contact force F is a function of the beam deflection. The contact force F will be a linear function of q if there were no stitches or delamination propagation. However in the present case it will be a nonlinear function. Once $F(q)$ is determined, then the equation of motion Equation 4.1a-4.1-c can be numerically integrated to obtain $q(t)$. From $q(t)$ one can compute the impact force history $F(t)$ using the F-q relation. In the following section we discuss the procedure for determining the F-q relation in a stitched delaminated beam.

4.2.1 Relation between Contact Force and Beam Deflection

The problem to be solved in this section is depicted in Figure 4-2. Because of symmetry only one half of the beam will be analyzed. The problem is to find the relation between transverse force F and deflection q at the center of the beam in the delaminated stitched beam. Further the energy release rate G at the crack tip needs to be computed also. In the numerical simulation the crack will be propagated by a small distance (symmetrically on both sides) if the G exceeds the Mode II fracture toughness G_{IIC} of the parent laminated material system.

First we will provide an overview of the procedures to be followed. Since the structure is symmetric we can analyze the right half of the beam as shown in Figure 4-3. The crack

[illegible]

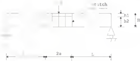

Figure 4 2 A delaminated beam with stitches subject to impact load F

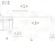

Figure 4 3 Right half side of specimen in Figure 4 2

The right half beam can be divided into three elements Element 1, Element 2 and Element 3. In Figure 4-3 they are denoted as <1>, <2> and <3>. Free body diagrams of the three elements are shown in Figure 4.4. At each end of the element there are three displacements, u, w, and ψ, and three corresponding forces, F_x, F_z, and C. The u and w are the displacements in the x and z directions and ψ is the rotation of the cross section. In the list of forces C represents the couple corresponding to the rotation ψ. We use the Timoshenko beam theory in modelling the beams. The equations of equilibrium of a general element are given in the Appendix. These equations can be easily solved as shown in the Appendix to obtain a relation between the six forces acting at the two ends of the element and the six corresponding displacements. In order to relate the forces in the three different elements we use force and moment equilibrium equations, and compatibility equations at the junctions (nodes) where the elements meet. Further, the boundary conditions at the ends of the beam can also be implemented. This procedure is similar to assembling elements in the Finite Element Method except the stiffness matrix of each element is obtained exactly by solving the differential equations of equilibrium. The forces and displacements in each element are shown in Figure 4.4. It should be noted that F is the contact force acting on the beam, and because of symmetry F/2 is assumed to act at Node 1 in Element 1. The compatibility relation for the axial displacements at the junction of all three elements is depicted in Figure 4 5

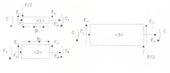

Figure 4 4 Free body diagrams of part <1>, <2>, <3>

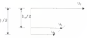

Figure 4 5 Compatibility of displacement
in axial direction at joint position

The force and moment equilibrium equations, the compatibility equation and boundary conditions are as follows [illegible]rce and moment equilibrium equ[illegible]

$$F_{x2} + F_{x4} + [illegible] \quad (4.2)$$

$$F_{z2} + F_{z4} [illegible] \frac{P}{2} \quad (4.3)$$

$$F_{x2} + F_{x4} + F_{x5} = 0 \quad (4.4)$$

$$C_2 + C_4 + C_5 + F_{x2}\frac{h_2}{2} - F_{x4}\frac{h_1}{2} = 0 \quad (4.5)$$

Compatibility equations at the joints

$$u_2 = u_5 + \frac{h_2}{2}\psi_5 \quad (4.6)$$

$$u_4 = u_5 - \frac{h_1}{2}\psi_5 \quad (4.7)$$

$$w_2 = w_4 = w_5 \quad (4.8)$$

$$\psi_2 = \psi_4 = \psi_5 \quad (4.9)$$

Boundary conditions

$$u_1 = u_3 = 0 \quad (4.10)$$

$$\psi_1 = \psi_3 = 0 \quad (4.11)$$

$$w_1 = w_3 \quad (4.12)$$

$$w_6 = F_{x6} = C_6 = 0 \quad (4.13)$$

[illegible] and [illegible] directions and transverse [illegible], [illegible] is moment of a beam. Odd indices [illegible] 1, [illegible] the left end node of each element and even indices (i = [illegible] 4, 6) correspond to the right end nodes. Expressions of F_{xi}, F_{zi} and C_i are derived in the Appendix

After implementing the aforementioned element equilibrium conditions and displacement compatibility conditions at the nodes, a compact set of 5 equations are obtained for the five displacements w_1, u_5, w_5, ψ_5, and ψ_6 as shown in Equation 4 14

$$\begin{bmatrix} k_{11} & k_{12} & k_{13} & k_{14} & k_{15} \\ k_{21} & k_{22} & k_{23} & k_{24} & k_{25} \\ k_{31} & k_{32} & k_{33} & k_{34} & k_{35} \\ k_{41} & k_{42} & k_{43} & k_{44} & k_{45} \\ k_{51} & k_{52} & k_{53} & k_{54} & k_{55} \end{bmatrix} \begin{Bmatrix} w_1 \\ u_5 \\ w_5 \\ \psi_5 \\ \psi_6 \end{Bmatrix} = \begin{Bmatrix} f_1 \\ f_2 \\ f_3 \\ f_4 \\ f_5 \end{Bmatrix} \tag{4 14}$$

The stiffness coefficients k_{ij} (i=1,5, j=1,5) and the generalized forces f_1..f_5 on the right hand side of Equation 4 14 are given in Equation 4.14-a

$$\mathbf{k}_{12} = \mathbf{k}_{15} = \mathbf{k}_{21} = \mathbf{k}_{23} = \mathbf{k}_{25} = \mathbf{k}_{51} = \mathbf{k}_{52} = 0$$

$$\mathbf{k}_{11} = \frac{1}{\mathbf{B}_1\mathbf{a}} + \frac{1}{\mathbf{B}_2\mathbf{a}}$$

$$k_{13} = k_{31} = -\frac{1}{B\,a} - \frac{1}{B\,a}$$

$$k_{14} = k_{41} = -\frac{1}{2B_1} - \frac{1}{2B_2}$$

$$k_{22} = \frac{A_1E_1}{a} + \frac{A_2E_2}{a}$$

$$k_{24} = k_{42} = \frac{A_1E_1h_2}{2a} - \frac{A_2E_2h_1}{2a}$$

$$k_{33} = \frac{1}{B_1a} + \frac{1}{B_2a} + \frac{1}{B_3L}$$

$$k_{34} = k_{43} = \frac{1}{2B_1} + \frac{1}{2B_2} - \frac{1}{2B_2}$$

$$k_{35} = k_{53} = -\frac{1}{2B_3}$$

$$k_{44} = \frac{E_1I_1}{a} + \frac{a}{4B_1} + \frac{E_2I_2}{a} + \frac{a}{4B_2} + \frac{E_3I_3}{L} + \frac{L}{4B_3} + \frac{A_1E_1h_2^2}{4a} + \frac{A_2E_2h_1^2}{4a}$$

$$k_{45} = k_{54} = \frac{L}{4B_3} - \frac{E_3I_3}{L}$$

$$k_{55} = \frac{E_3I_3}{L} + \frac{L}{4B_3}$$

$$f_1 = -\frac{F}{2} + \frac{p_0h_1a^2}{24E_1I_1B_1} + \frac{p_0h_2a^2}{24E_2I_2B_2}$$

$$f_2 = \frac{p_0h_2a^2}{24E_2I_2B_2} - \frac{p_0h_1a^2}{24E_1I_1B_1}$$

$$f_4 = \frac{p_0h_1a^3}{48E_1I_1B_1} - \frac{p_0h_2a^3}{48E_2I_2B_2}$$

$$f_3 = f_5 = 0 \qquad (4.14-a)$$

The expressions for B_1, B_2, B_3 in Equation 4.14 are as follows:

$$B_1 = \frac{1}{G_1 A_1} + \frac{a^2}{12 E_1 I_1}$$

$$B_2 = \frac{1}{G_2 A_2} + \frac{a^2}{12 E_2 I_2}$$

$$B_3 = \frac{1}{G_3 A_3} + \frac{L^2}{12 E_3 I_3}$$

Note that E_i and G_i are the equivalent Young's modulus and shear modulus, respectively, and A and I are area of cross section and moment of inertia of the corresponding beam element.

In Equation 4.14 the forces $f_2, \ldots, f_6$ are known. The force f_1 that is related to the contact force F is the unknown. On the other hand the deflection w_1 (same as the variable q used in impact equations) can be treated as known, and the other five displacements are unknowns. Thus we have five equations for five unknowns. The equations can be solved for a given w_1 to determine f_1 or the contact force-displacement F-q relations can be developed.

The flowchart in Figuation 4.6 describes the procedure used in developing the F-q relations. Further at each displacement increment the energy release rate G is computed using the procedure explained in the next paragraph. If the value of G exceeds the Mode II fracture toughness G_{IIc}, the length of the delamination is increased by a small amount. The numerical value of the extension is arrived by a trial and error method until G equals G_{IIc} for that deflection increment.

In order to compute the G we used the strain energy density method derived by Sankar [52]. This method is very much suitable for the present model as the force and moment resultant ahead and behind the crack tip can be obtained in closed-form from the solution of the differential equations of equilibrium and the energy density values thus calculated does not have any numerical errors. Consider the three elements surrounding the crack tip as shown in Figure 4.3. There are two (Elements 1 and 2) behind the crack tip and one ahead of the crack tip (Element 3). The G is derived as

$$G = \frac{1}{B}\left(U_L^1 + U_L^2 - U_L^3\right) \tag{4.15}$$

here U_L represents the strain energy density (strain energy per unit length of the beam), the superscripts (1) and (2) denote the cross sections immediately behind the crack tip and (3) denotes the cross section immediately ahead of the crack tip and B is the width of the beam in the y-direction.

The strain energy density in terms of force and moment resultants is given by

$$U_s = \frac{1}{2}\left(\frac{F^2}{EA} + \frac{M^2}{EI} + \frac{V^2}{GA}\right) \tag{4.16}$$

where *F*, *M* and *V* are the axial force, bending moment and shear force resultants; *EA*, *EI* and *GA* are the equivalent axial, flexural and shear rigidities of the beam cross section.

4.2.2 Impact Response

After computing the *F*-*q* relation for a beam, the impact equations (Equation 4.1-c) can be solved numerically. The *F*-*q* relations were stored in a spread sheet program (Excel™). The expression for *F(q)* on the RHS of Equation 4.1-a can be approximated by a linear interpolation in each small integration step as

$$F(q) = F_i + \frac{F_f - F_i}{(q_f - q_i)}(q - q_i) \tag{4.17}$$

where q_i and q_f are impactor initial and final displacements and F_i and F_f are initial and final contact force in each increment.

From equation [illegible] , the relation between contact force F and velocity V can be derived as follows.

$$M\frac{d}{dt}\left(\frac{dq}{dt}\right)=-F(q) \qquad (4.18-a)$$

where

$$\frac{dq}{dt}=V \qquad (4.18-b)$$

Substituting Equation 4.18-b into Equation 4.18-a and a new equation Equation 4.18-c relating the contact force $F(q)$ and the impact velocity V can be obtained.

$$M\frac{dV}{dq}\frac{dq}{dt}=-F(q) \qquad (4.18-c)$$

Substituting Equation 4.18-b into Equation 4.18-c and integrating both sides of the equation, the relation between V and $F(q)$ can be derived as:

$$\frac{1}{2}M(V_2^2-V_1^2)=-\int_{q_1}^{q_2}F(q)dq \qquad (4.18-d)$$

Substituting Equation 4.17 into Equation 4.18-d the velocity can be expressed in following form

$$V_2=\sqrt{V_1^2-\frac{1}{M}(q_2-q_1)(F_1+F_2)} \qquad (4.19)$$

where V_1 and V_2 are initial and final velocities in each step

The corresponding impact time can be derived using Equation 4.18-b by assuming that the impact velocity in each step varies linearly

$$V(q) = V_1 + \frac{V_2 - V_1}{q_2 - q_1}(q - q_1) \qquad (4.20-a)$$

here q_1 and q_2 are impactor initial and final displacements in each step. Integrating Equation 4.18-b and then substituting Equation 4.20-a we derive the following integral equation

$$\int_{t_1}^{t} dt = \int_{q_1}^{q_2} \frac{dq}{V(q)} = \int_{q_1}^{q_2} \frac{dq}{V_1 + \frac{(V_2 - V_1)(q - q_1)}{(q_2 - q_1)}} \qquad (4.20-b)$$

Integrating Equation 4.20-b an expression for time t_2 can be obtained as

$$t_2 = t_1 + \frac{(q_2 - q_1)}{(V_2 - V_1)} \ln \frac{V_2}{V_1} \qquad (4.20-c)$$

here t_1 and t_2 are initial and final time in each step. Equation 4-20-c provides the *q*-t relation for the impact problem. From that using *F*-q relations, we can obtain the *F*-t relation or the impact force history. Since we know the delamination length at each displacement in the static problem, i.e., a-q relation, we can translate that into a-t relation, and thus the propagation of delamination can be followed.

4.3 Numerical Example, Results, and Discussion

The specimen dimension and material properties used in the impact simulation are as follows. Initial uncracked length L_c=74.2 mm, initial crack length a_0=27.4 mm, beam width B=25.4 mm, equivalent Young's modulus E_{eq}=90.375 GPa, equivalent shear modulus G_{xy}=6.4GPa. Stitching material is 3570 denier glass yarn. Nine different examples were studied. In these examples, the impactor mass, impact velocity, position of the delamination in the thickness direction and the Mode II fracture toughness G_{IIc} were varied. The parameters used in these examples are listed in Table 4.1.

In Table 4.1 H is the total thickness of the beam and h_1 is the distance of delamination from the top surface (impact surface). For each example three different cases - beam without stitching, 16 ssi stitches, and 64 ssi stitches - were considered. Thus a total of 27 impact simulations were performed. The simulations were stopped when the contact force becomes equal to zero denoting the contact between the impactor and the beam has ceased. In two cases (Example 2, no stitches and 16 ssi stitches) the simulation has to be stopped when the delamination propagated all the way to the ends of the beam.

Table 4.1 Various parameters used in numerical examples

EXAMPLE NO.	M_0 (kg)	V_0 (m/s)	T (J)	POSITION OF DELAMINATION (h_1/H)	G_{IIC} (N/m)
1	5	1.5	5.625	0.5	530
2	5	1.5	5.625	0.5	300
3	1.25	3	5.625	0.5	530
4	2.5	1.5	2.813	0.5	530
5	2.5	1.5	2.813	0.5	300
6	5	1.5	5.625	0.25	530
7	5	1.5	5.625	0.25	300
8	2.5	1.5	2.813	0.25	530
9	2.5	1.5	2.813	0.25	300

Note: M_0 (Impactor Mass), V_0 (Impact velocity), T (Kinetic energy)

From the static analysis we obtain the load-deflection relation (F-q) and the delamination-deflection relation (a-q). Sample F-q relations for Example 1 are shown in Figure 4.7. The F-q relation is linear until the crack begins to propagate. It may be noted that the load at which the crack begin to propagate is almost the same for all three cases (no stitches, 16 ssi, and 64 ssi stitches). After that the curves take different shapes depending on the stitch density. The maximum load that the beam can carry vary much depends on the stitch density. The 64 ssi beam carries about 50% more load than the unstitched beam. The unloading was assumed to be linear and hence the unloading curve was a straight line joining the point [illegible] unloading and the origin. This assumption is validated by the Mode II experiments conducted by Sharma and Sankar [46].

Another interesting result that can be deduced from the static load-deflection curve is the apparent fracture toughness of stitched laminates. The area enclosed by the load-deflection diagram (Fig. 4.7) denotes the work of fracture. Since we know the extent of delamination propagation we can compute the apparent fracture toughness from

$$G_{IIc} = \frac{\Delta W}{\Delta A}$$

here ΔW is the work done and ΔA is the new delamination surface created. The apparent fracture toughness for various cases is presented in Table 4.2 along with that for unstitched laminates. The numbers in parentheses are the percentage increase in apparent fracture toughness. It may be seen that the percentage increase in G_{IIc} is higher for laminates with lower fracture toughness.

The results for each impact analysis include the complete impact force history (F-t) and the delamination propagation history (a-t). A sample impact force history is shown in Figure 4.8. In general, stitched beams carry more impact force, provided the impact energy is sufficient to cause delamination propagation. For low impact energies, the impact force history will be identical in stitched and unstitched beams, because the stitches come into effect only when there is sufficient energy to propagate the delamination

Table 4.2 Comparisons of G_{IIc}

CASE	G_{IIc} (N/m)	G_{IIc} for 16ssi	G_{IIc} for 64ssi
1	530	595 (12%)	707 (33%)
2	300	344 (15%)	430 (43%)

The results presented in Table 4.3 show for each case impact energy, G_{IIc} of the parent material system, the contact force F_i at which the delamination began to propagate, the final crack length a_{max} and the maximum contact force F_{max} during the impact event. The extent of delamination propagation is also shown in the bar charts in Figures 4.9 and 4.10. Figure 4.9 considers the examples wherein the G_{IIc} = 530 J/m^2 and Figure 4.10 corresponds to G_{IIc}=300 J/m^2.

There are many interesting observations that can be made from the results presented in Table 4.3. The contact force at which the delamination propagates is almost the same in unstitched and stitched beams. This initiation force depends only on the G_{IIc} and the position of the crack

$h1/H$). Thus [illegible] on impact parameters [illegible] impact energy.

In general the extent of crack propagation at the end of the impact event is the least in the 64 ssi beam and the highest in the unstitched beams The result for 16 ssi beams are somewhere in between. This can also be observed readily from the bar charts in Figures 4 9 and 4 10 However the amount of delamination propagation depends also on the impact energy, G_{IIc} and $h1/H$. Stitching is very effective in the beam with lower inherent fracture toughness In Example 2 (G_{IIc} = 300 N/m) the crack propagates all the way to the ends of the beam in the unstitched and 16 ssi specimens, whereas the crack propagated up to a=59.4 mm in the 64 ssi beam. In Example 1 (G_{IIc} = 530 N/m) the stitches were able to reduce the delamination extension by about 6 - 12 mm

Stitches are also more effective when the crack is in the middle plane of the laminate ($h1/H$=0.5) compared to the cases wherein the crack is near the top surface of the beam ($h1/H$=0 25). This can be explained as follows. In an undelaminated beam the shear stresses are higher at the midplane (1 5 times the average shear stress) compared to the plane at 1/4 distance from the top Thus when the delamination is at the midplane the tendency for propagation is much higher In fact the energy release rate G is higher for midplane delaminations. Thus the stitches play a very useful role in preventing crack propagation. This situation is similar to the effectiveness of stitches for various G_{IIC}'s

The stitches become more effective at higher impact energies when the propensity for crack propagation is also higher. Comparing Examples 1 and 4 in Figure 4.9 one can see this phenomenon. In Example 4 the impact energy was very low so that stitching was not necessary. However in Example 1 the effectiveness of stitch density could be inferred

From the above discussion we can arrive at the following conclusions:

1. Static simulations of delaminated stitched beam provide an estimate of the apparent fracture toughness of the stitched laminates. The stitch density significantly affects the increase in apparent fracture toughness. The percentage increase is more for laminates with lower inherent fracture toughness.
2. The impact force at which the delamination begins to grow is not dependent on stitching. However after the delamination growth is initiated stitches come into play, and the extent of delamination growth depends on the stitching parameters. In general the extent of crack propagation at the end

of an impact event is small for higher stitch densities.

3. Stitching is effective when the impact energies are higher and the propensity for delamination growth is also higher.
4. Stitching is more effective when the delamination is at the center.

Table 4.3 Contact force vs crack length in various examples

EXAMPLE	h /H	CASE	F (N)	a_{max} (mm)	F_{max} (N)
Example 1 T=5.6125J G_{IIc}=530N/m	0.5	No stitch	553	56.4	645
		16 ssi	562	50.4	678
		64 ssi	577	44.4	713
Example 2 T=5.6125J G_{IIc}=300N/m	0.5	No stitch	416	101.4	431
		16 ssi	423	101.4	465
		64 ssi	438	59.4	679
Example 3 T=5.6125J G_{IIc}=530N/m	0.5	No stitch	553	56.4	645
		16 ssi	562	50.4	678
		64 ssi	577	44.4	713
Example 4 T=2.813J G_{IIc}=530N/m	0.5	No stitch	545	27.4	545
		16 ssi	546	27.4	546
		64 ssi	548	27.4	546
Example 5 T=2.813J G_{IIc}=300N/m	0.5	No stitch	416	49.4	478
		16 ssi	425	44.4	496
		64 ssi	438	39.4	517
Example 6 T=5.6125J G_{IIc}=530N/m	0.25	No stitch	569	47.4	708
		16 ssi	571	46.4	711
		64 ssi	578	44.4	721
Example 7 T=5.6125J G_{IIc}=300N/m	0.25	No stitch	428	74.4	646
		16 ssi	431	67.4	667
		64 ssi	437	60.4	692
Example 8 T=2.813J G_{IIc}=530N/m	0.25	No stitch	547	27.4	547
		16 ssi	547	27.4	547
		64 ssi	549	27.4	549
Example 9 T=2.813J G_{IIc}=300N/m	0.25	No stitch	428	43.4	507
		16 ssi	431	41.4	511
		64 ssi	437	40.4	518

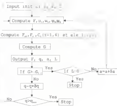

a=crack length
L=uncrack length
F=impact force
q=deflect at center point
G=energy release rate

Figure 4.6 Flow chart for computing the F-q relation

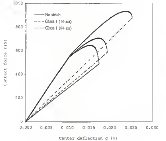

Figure 4.7 Contact force F vs. center deflection q (G_{IIc}=530J/m^2)

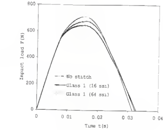

Figure 4.8 Impact load F vs. time t

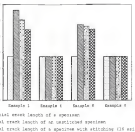

Figure 4 9 Crack growth in different examples
(G_{IIC}=530J/m^2)

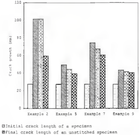

Figure 4 10 Crack growth in different examples (G_{IIC}=300J/m^2)

CHAPTER [illegible]
CONCLUSIONS AND FUTURE WORK

[illegible].1 Summary

In this dissertation analytical and finite element methods are used to investigate the effects of through-the-thickness stitching on the mechanical behavior of delaminated composite laminates. In particular the buckling and post-buckling response and low velocity impact response of delaminated composites are studied. These two loading modes were selected as they are very detrimental to effective functioning of composites containing delaminations.

The analytical models use the Raleigh Ritz method in which stitches are modeled as smeared foundation springs. The finite element models have the capability of modeling individual stitches. The low-velocity impact response calculations use the static load deflection behavior of the stitched composite beam.

From the results presented in the previous chapters the following conclusions can be reached:

1. From the analytical models a single non-dimensional parameter K' was identified

$$K = \frac{A_s E_s}{2h} \frac{NB}{E}$$

   It may be noted that K' is actually the ratio of the stitch stiffness and the equivalent Young's modulus of the beam. Thus one needs to use high density stitches with stiffer yarn material if the flexural modulus of the laminate is also higher. It is found that stitching increases the buckling load, and reduces the energy release rate at the crack-tip

2. The FE models also support the conclusions of the analytical models. The strains in the stitches depend on the axial stiffness of the stitches, and they determine if the stitch will break during the post-buckling process and thus reduce the effectiveness of stitching

3. From the static simulations of a delaminated beam it is found that the percentage increase in apparent fracture toughness is more for laminates with lower inherent fracture toughness. The impact force at which the delamination begins to grow is not dependent on stitching. However the extent of delamination growth depends on the stitching parameters. Stitching is

effective when the impact energies are higher and when the delamination is at the center.

5.2 Suggestions for Future Work

The present research assumed a single central delamination. The models, especially the FE models, can be extended to beams with multiple delaminations. Further, FE models can handle laminated plates with stitching and other forms of translaminar reinforcements. Since it will not be possible to model individual stitches in larger plates, equivalent stitch parameters such as foundation spring constants may have to be used. More complex constitutive relations based on experimental observations can be used to model the stitch yarn or other translaminar reinforcements.

Since stitching results in increased cost and weight, optimization studies can be undertaken to determine the effective stitch materials and stitch pattern in the design of laminated composite structures.

APPENDIX
DERIVATION OF FORCE-DISPLACEMENT RELATIONS IN THE BEAM ELEMENT

In this appendix the derivations for external forces F_{xi}, F_{zi} and moments C described in Chapter 4 are given.

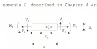

Figure A.1 Free body diagram in part <1>

Consider Part <1> of the beam shown in Figure A.1. In Figure A.1 P_i, V_i, and M_i (i=1,2) are internal force and moment. p_s is shear force provided by stitches. The relations between external forces and internal force resultants at left side of a beam and right side of a beam are given as follows:

$$F_{x1} = -P_1$$

$$F_{z1} = -V_1$$

$$C = -M_1 \qquad (A.1)$$

$$F_{X2} = P_2$$

$$F_{Z2} = V_2$$

$$C_2 = M_2 \qquad (A.2)$$

Now we consider the internal force P in the axial direction shown in Figure A 2

Figure A 2 Free body diagram in axial direction

The differential equations of equilibrium are.

$$A_1E_1\frac{d^2u}{dx^2} = \frac{dP}{dx} - p_1 \qquad (A.3)$$

$$A_1E_1\frac{du}{dx} = P \qquad (A.4)$$

Here A_1 is area of cross section of part <1>, E_1 is young's modulus of part <1> Substituting boundary condition at x=0, u=u$_1$, at x=a, u=u$_2$ into Equations A.3 and A.4 and consider the equations in Equations A 1 and A 2, we have following expressions of F_{X1} and F_{X2}:

$$F_{x1} = \frac{A_1E_1}{a}(u_1 - u_2) + \frac{p_s a}{2} \tag{A5}$$

$$F_{x2} = \frac{A_1E_1}{a}(u_2 - u_1) + \frac{p_s a}{2} \tag{A6}$$

We consider the segment shown in Figure A.3 for deriving the expressions for F_{xi} and C_i ($i=1,2$).

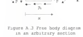

Figure A.3 Free body diagram in an arbitrary section

The moment and force resultants *M* and *V* in an arbitrary cross section can be expressed as

$$E_1 I_1 \frac{d\psi}{dx} = M = M_1 + V_1 x - p_s x \frac{h_1}{2} \tag{A7}$$

$$G_1 A_1 (\psi + \frac{dw}{dx}) = V = V_1 \tag{A8}$$

Here I_1 is moment of inertia and G_1 is shear modulus of part <1>

At $x=0$

$$w = w_1 \quad \psi = \psi_1 \quad V = V_1 \quad M = M_1 \tag{A.9}$$

At $x=a$

$$w = w_2 \quad \psi = \psi_2, \quad V = V_2, \quad M = M_2 \tag{A.10}$$

Solving Equations A.7 and A.8 and using the boundary conditions in Equations A.9 and A.10, we obtain relations between V, M and w_i, θ_i. Then F_{zi} and C_i can be expressed in terms of w, θ as

$$F_{z1} = \frac{1}{A_1 a}(w_1 - \frac{a}{2}\psi_1 - w_2 - \frac{a}{2}\psi_2 - \frac{p_0 h_1 a^3}{24E_1 I_1}) \tag{A.11}$$

$$F_{z2} = \frac{1}{A_1 a}(-w_1 + \frac{a}{2}\psi_1 + w_2 + \frac{a}{2}\psi_2 + \frac{p_0 h a^3}{24E I_1}) \tag{A.12}$$

$$C_1 = -\frac{w_1}{2A_1} + \psi_1(\frac{E_1 I_1}{a} + \frac{a}{4A_1}) + \frac{w_2}{2A_1}$$

$$+\psi_2(\frac{a}{4A_1} - \frac{E_1 I_1}{a}) + \frac{p_0 h_1 a^3}{48E_1 I_1 A_1} - \frac{p_0 h a}{4} \tag{A.13}$$

$$C_2 = \frac{w_1}{2A_1} + \psi_1(-\frac{E_1 I_1}{a} + \frac{a}{4A_1}) + \frac{w_2}{2A_1}$$

$$+\psi_2(\frac{a}{4A_1} + \frac{E_1 I_1}{a}) + \frac{p_0 h_1 a^3}{48E_1 I_1 A_1} - \frac{p_0 h_1 a}{4} \tag{A.14}$$

where

$$A_1 = \frac{1}{G_1 A_1} + \frac{a^2}{12 E_1 I_1}$$

Free body diagram of portion <2> is shown in Figure A.4.

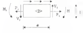

Figure A.4 Free body diagram in part <2>

The procedure for deriving the expressions for F_{xi}, F_{zi}, and C_i (i=3,4) is similar to that one in part <1>, therefore the derivation is omitted here

$$F_{x3} = -\frac{p_0 a}{2} + \frac{A_2 E_2}{a}(u_3 - u_4) \tag{A.15}$$

$$F_{x4} = -\frac{p_0 a}{2} + \frac{A_2 E_2}{a}(u_4 - u_3) \tag{A.16}$$

$$F_{z4} = \frac{1}{A_2 a}\left(\frac{p_0 h_2 a^3}{24 E_2 I_2} - w_3 + \frac{\psi_3 a}{2} + w_4 + \frac{\psi_4 a}{2}\right) \tag{A.17}$$

$$F_{z3} = \frac{1}{A_2 a}\left(-\frac{p_0 h_2 a^3}{24 E_2 I_2} + w_3 - \frac{\psi_3 a}{2} - w_4 - \frac{\psi_4 a}{2}\right) \tag{A.18}$$

$$C_3 = \frac{w_3}{2A_2} + \psi_3\left(\frac{a}{4A_2} + \frac{E_2 I_2}{a}\right) + \frac{w_4}{2A_2}$$

$$+\psi_4\left(\frac{a}{4A_2} - \frac{E_2 I_2}{a}\right) + \frac{p_3 h_2 a^3}{48E_2 I_2 A_2} - \frac{p_6 h_2 a}{4} \qquad (A19)$$

$$C_4 = -\frac{w_3}{2A_2} + \psi_3\left(\frac{a}{4A_2} - \frac{E_2 I_2}{a}\right) + \frac{w_4}{2A_2}$$

$$+\psi_4\left(\frac{a}{4A_2} + \frac{E_2 I_2}{a}\right) + \frac{p_3 h_2 a^3}{48E_2 I_2 A_2} - \frac{p_6 h_2 a}{4} \qquad (A20)$$

A_2 is area of cross section, E_2 is Young's modulus and G_2 is shear modulus in part <2> and Λ_2 is given by

$$\Lambda_2 = \frac{1}{G_2 A_2} + \frac{a^2}{12E_2 I_2}$$

The free body diagram of part <3> is shown in Figure A.5

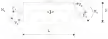

Figure A.5 Free body diagram in part <3>

We can derive expressions for F_{xi}, F_{zi}, and C $(i=5,6)$ as shown below. The procedure for deriving these expressions is similar to that one in part <1>.

$$F_{x5}=\frac{A_3E_3}{L}(u_5-u_6) \tag{A.21}$$

$$F_{x6}=\frac{A_3E_3}{L}(u_6-u_5) \tag{A.22}$$

$$F_{z5}=\frac{w_5}{A_3L}-\frac{\psi_5}{2A_3}-\frac{w_6}{A_3L}-\frac{\psi_6}{2A_3} \tag{A.23}$$

$$F_{z6}=-\frac{w_5}{A_3L}+\frac{\psi_5}{2A_3}+\frac{w_6}{A_3L}+\frac{\psi_6}{2A_3} \tag{A.24}$$

$$C_5=-\frac{w_5}{2A_3}+(\frac{E_3I_3}{L}+\frac{L}{4A_3})\psi_5+\frac{w_6}{2A_3}+(-\frac{E_3I_3}{L}+\frac{L}{4A_3})\psi_6 \tag{A.25}$$

$$C_6=-\frac{w_5}{2A_3}+(-\frac{E_3I_3}{L}+\frac{L}{4A_3})\psi_5+\frac{w_6}{2A_3}+(\frac{E_3I_3}{L}+\frac{L}{4A_3})\psi_6 \tag{A.26}$$

A is area of cross section, E_3 is Young's modulus and G_3 is shear modulus in part <3>, and A_3 is given by

$$A_3=\frac{1}{G_3A_3}+\frac{L^2}{12E_3I_3}$$

[illegible]

[1] Chai, H., Babcock, [illegible] Dimension Modeling of [illegible] Delamination Buckling," International Journal of [illegible] Structures 17(11), 1982, [illegible]

[2] Yin, W.L., and Wang, J.T.S., "The Energy Release [illegible] in the Growth of a One-Dimension Delamination," Journal of Applied Mechanics 51, Dec 1983, 939-941

[3] Whitcomb, J.D., "Finite Element Analysis of [illegible] Related Delamination Growth," Journal of Composite Materials 15(9), 1981, 403-426.

[4] Sheinman, I., and Soffer, M., "Post-buckling Analysis of Composite Delaminated Beams," International Journal of Solids and Structures 27(5), 1991, 639-646.

[5] Kardomateas, G.A., and Schmueser, D.W., "Buckling and Post-buckling of Delaminated Composites under Compressive Loads Including Transverse Shear Effects," AIAA Journal 26(3), 1988, 337-343

[6] Kardomateas, G.A., "Large Deformation Effects in the Post-buckling Behavior of Composites with Thin Delaminations," AIAA Journal 27(5), 1989, 624-631

[7] Chen, H., "Shear Deformation Theory for Compressive Delamination Buckling and Growth," AIAA Journal 29(5), 1991, 813-819.

[8] Chen, H., "Transverse Shear Effects on Buckling and Post-buckling of Laminated and Delaminated Plates," AIAA Journal 31(1), 1993, 163-169

[9] Davidson, B.D., and Krafchak, T.M., "Analysis of Instability-Related Delamination Growth Using a Crack tip Element," AIAA Journal 31(11), 1993, 2130-2136.

[10] Davidson, B.D., "Energy Release Rate Determination for Edge Delamination under Combined In-Plane, Bending and Hygrothermal Loading. Part II: Two Symmetrically Located Delaminations," Journal of Composite Materials 28(14), 1994: 1371-1392.

[11] Davidson, B.D., and Krafchak, T.M., "A Comparison of Energy Release Rates for Locally Buckled Laminates Containing Symmetric and Asymmetrically Located Delaminations," Journal of Composite Materials 29(6), 1995: 701-713.

[12] Kyoung, W., and Kim, C., "Delamination Buckling and Growth of Composite Laminated Plates with Tranverse Shear Deformation,' Journal of Composite Materials 29(15), 1995: 2047-2068.

[13] Lee, J., Gurdal, Z., and Griffin Jr., O. H., "Post-buckling of Laminated Composites with Delaminations," AIAA Journal 33(10), 1995: 1963-1970.

[14] Yin, W.L., and Fei, Z., "Delamination Buckling and Growth in a Clamped Circular Plate," AIAA Journal 26(4), 1988: 438-445.

[15] Whitcomb, J.D., and Shivakumar, K.N., "Strain Energy Release Rate Analysis of Plates with Post-buckled Delaminations," Journal of Composite Materials 23, July 1989: 714-733.

[16] Suemasu, H., "Effect of Multiple Delaminations on Compressive Buckling Behaviors of Composite Panel," Journal of Composite Materials 27(12) 1993: 1172-1192.

[17] Naganarayana, B.P., and Atluri, S.N., "Energy-Release-Rate Evaluation for Delamination Growth Prediction in a Multi-Plate Model of a Laminate Composite," Computational Mechanics 15, 1995: 443-459.

[18] Naganarayana, B.P., and Atluri, S.N., "Strength Reduction and Delamination Growth in Thin and Thick Composite Plates under Composite Loading," Computational Mechanics 16, 1996: 170-189.

[19] Shen, H., and Williams, F.W., "Post-buckling Analysis of Imperfect Laminated Plates under Combined Axial and Thermal Loads," Computational Mechanics 17, 1996: 226-233.

[20] Kiug, J., Wu, X.X., and Sun, C.T., "Efficient Modeling of Post-buckling delamination Growth in Composite Laminates Using Plate Elements," AIAA Journal 34(1), 1996: 178-184.

[21] Graves, J.M., and Kantz, J.S., "Initiation and Extent of Impact Damage in Graphite/Epoxy and Graphite/Peak Composites," Proceedings of the AIAA/ASME/ASCE/AHS 28th Structures, Structural Dynamics, and Materials Conference, AIAA, Reston, Virginia, 1988: 967-976.

[22] Clark, G., "Modeling of Impact Damage in Composite Laminate," Composites 20(3), 1989: 209-214.

[23] Grady, J.H., and Sun, C.T., "Dynamic delamination Crack Propagation in a Graphite/Epoxy Laminate," Composite Materials: Fatigue and Fracture, ASTM STP 907, 1986: 5-31.

[24] Grady, J.E., and Depaola, K.J., "Measurement of Impact Induced Delamination Buckling in Composite Laminates," Dynamic Failure, Procaedings of the 1987 SEM Fall, Society for Experimental Mechanics, Bethel, CT, 1987: 250-255.

[25] Choi, H.Y., Wu, H.T., and Chang, F.K., "A New Approach toward Understanding Damage Mechanism and Mechanics of Laminated Composites Due to Low-Velocity, Part I-Experiments," Journal of Composite Materials 25, Aug. 1991: 992-1011.

[26] Sankar, B.V., and Hu, S., "Dynamic Delamination Propagation in Composite Beams," Journal of Composite Materials 25, Nov. 1991: 1414-1426.

[27] Hu, S., "Dynamic Delamination Propagation in Composite Beams under impact," PhD dissertation, University of Florida, Gainesville, Florida, 1990.

[28] Razi, H., and Kobayashi, A.S., "Delamination in Cross-Ply Laminated Composite Subjected to Low-Velocity Impact," AIAA Journal 31(8), 1993: 1498-1502

[29] Sun, C.T., and Yih, C.J., "Quasi-Static Modeling of Delamination Crack Propagation in Laminates Subjectad to Low-Velocity Impact," Composites Science and Technology 54, 1995: 185-191

[30] Wang, H., and Vu-Khanh, T., "Fracture Mechanics and Mechanisms of Impact-Induced Delamination in Laminated

Composites," Journal of Composite Materials 29(2), 1995: 156-178.

[31] Kwon, Y.S., and Sankar, B.V., "Indentation-Flexure and Low-Velocity Impact Damage in Graphite Epoxy Laminates," Journal of Composites Technology & Research 15, 1993: 101-111

[32] Kwon, Y.S., and Sankar, B.V., "Indentation-Flexure and Low-Velocity Impact Damage in Graphite/Epoxy Laminates," NASA Contractor Report 187624, 1992.

[33] Sankar, B.V., "Low-Velocity Impact Response and Damage in Composite Materials," Fracture of Composites, E. Armanios, Ed., Transtech Publications, Ltd., Zurich, Switzerland, 555-582

[34] Sawyer, J.W., "Effect of Stitching on the Strength of Bonded Composite Single Lap Joints," AIAA Journal 23(11), 1985: 1744-1756.

[35] Su, K.B., "Delamination Resistance of Stitched Thermoplastic Matrix Composite Laminates," Thermoplastic Matrix Materials 5(2), 1991: 279-300.

[36] Dexter, H.B., and Funk, J., "Impact Resistance and Inter-laminar Fracture Toughness of Through-the-Thickness Reinforced Graphite/Epoxy," AIAA paper 86-1020-CP, 1986

[37] Pelstring, R.M., and Madan, R.C., "Stitching to Improve Damage Tolerance of Composites," 34th International SAMPE Symposium, Anaheim, CA., 1989: 1519-1528.

[38] Dransfield, K., Baillie, C., and Mai, Y., "Improving the Delamination Resistance of CFRP by Stitching-A Review," Composites Science and Technology 50, 1994: 305-317.

[39] Shu, D., and Mai, Y., "Delamination Bucking with Bridging," Composites Science and Technology 47, 1993: 25-33.

[40] Shu, D., and Mai, Y., "Effect of Stitching on Inter-laminar Delamination Extension in Composite Laminates," Composites Science and Technology 49, 1993: 165-171.

[41] Jain, L.K., and Mai, Y., "On the Effect of Stitching on Mode I Delamination Toughness of Laminated Composites," Composites Science and Technology 51, 1994, 331-345

[42] Jain, L.K., and Mai, Y., "Determination of Mode II Delamination Toughness of Stitched Laminated Composites," Composites Science and Technology 55, 1995, 241-253

[43] Chen, V.L., Wu, X.X., and Sun, C.T., "Effective Interlaminar Fracture Toughness in Stitched Laminates," Proceedings of the 8th annual technical meeting of American Society of Composites, Technomic Publishing Co., Lancaster, Pennsylvania, 1993, 453-462.

[44] Kang, T.J., and Lee, S.H., "Effect of Stitching on the Mechanical and Impact Properties of Woven Laminate Composite," Journal of Composite Materials 28(16), 1994, 1574-1587.

[45] Wu, E., and Liau, J., "Impact of Unstitched and Stitched Laminates by Line Loading," Journal of Composite Materials 28(17), 1994, 1640-1658.

[46] Sharma, S.K., and Sankar, B.V., "Effect of Through-the-Thickness Stitching on Impact and Inter-laminar Fracture Properties of Textile Graphite/Epoxy Laminates," NASA Contractor Report 195042, 1995.

[47] Sankar, B.V., and Sonik, V., "Modeling End-Notched Flexure Tests of Stitched Laminates," Proceedings of the 8th annual technical meeting of American Society of Composites, Technomic Publishing Co., Lancaster, Pennsylvania, 1995, 172-181.

[48] Dickinson, L.C., "Trans-Laminar-Reinforced (TLR) Composites," Department of Applied Science, PhD dissertation, College of William and Mary, Williamsburg, Virginia, 1997.

[49] Sankar, B.V., and Dharmapuri, S.M., "Analysis of a Stitched Double Cantilever Beam," Journal of Composite Materials 32(24), 1998, 2203-2225

[50] Jain, L.K., Dransfield, K.A., and Mai, Y., "Effect of Reinforcing Tabs on the Mode I Delamination Toughness of Stitched CFRPs," Journal of Composite Materials 32(22), 1998, 2016-2041.

[51] Glaessgen, E.H., Raju, I.S., and Poe, C.C., "Fracture Mechanics Analysis of Stitched Stiffener Debonding," AIAA Journal 20(22), 1998, 2633-2647

[52] Sankar, B.V., and Sonik, V., "Pointwise Energy Release Rate in Delaminated Plates", AIAA Journal 33(7), 1995, 1312-1318

[53] Anderson, T.L., Fracture Mechanics Fundamentals and Applications, 2nd Ed., CRC Press, Boca Raton, Florida, 1995.

[54] ABAQUS /Standard User's Manual (Version 5.7).

[55] ABAQUS Theory Manual (Version 5.7).

BIOGRAPHICAL SKETCH

Huasheng [illegible] born on July 17, 1966, in [illegible], People's Republic of China. She received a B.E. degree from Northwestern Polytechnical University in the Department of Aircraft in China in July 1987. Then she worked at [illegible] Institute of Aeronautical Engineering four years. She came to the United State for her graduate study in August 1991. She obtained her M.S. degree in Aerospace Engineering from the Department of Aerospace Engineering, Mechanics, and Engineering Science, University of Florida, in May 1994 and continued her Ph.D. study at the same department. She will receive her Ph.D. in December 1998.

I certify that I have read this study and that in my opinion it conforms to acceptable standards of scholarly presentation and is fully adequate, in scope and quality, as a dissertation for the degree of Doctor of Philosophy.

Bhavani V. Sankar, Chairman
Professor of Aerospace
Engineering, Mechanics, and
Engineering Science

I certify that I have read this study and that in my opinion it conforms to acceptable standards of scholarly presentation and is fully adequate, in scope and quality, as a dissertation for the degree of Doctor of Philosophy.

Nicolae D. Cristescu
Graduate Research Professor
of Aerospace Engineering,
Mechanics, and Engineering
Science

I certify that I have read this study and that in my opinion it conforms to acceptable standards of scholarly presentation and is fully adequate, in scope and quality, as a dissertation for the degree of Doctor of Philosophy.

Peter G. Ifju
Assistant professor of
Aerospace Engineering,
Mechanics, and Engineering
Science

I certify that I have read this study and that in my opinion it conforms to acceptable standards of scholarly presentation and is fully adequate, in scope and quality, as a dissertation for the degree of the Doctor of Philosophy

Edward K. Walsh
Edward K. Walsh
Professor of Aerospace Engineering, Mechanics, and Engineering Science

I certify that I have read this study and that in my opinion it conforms to acceptable standards of scholarly presentation and is fully adequate, in scope and quality, as a dissertation for the degree of Doctor of Philosophy

Reynaldo Roque
Reynaldo Roque
Professor of Civil Engineering

This dissertation was submitted to the Graduate Faculty of the College of Engineering and the Graduate School and was accepted as partial fulfillment of the requirements for the degree of Doctor of Philosophy

December 1993

M. J. Ohanian
Dean, College of Engineering

Winfred M. Phillips
Dean, Graduate School